Physics Letters B 842 (2023) 137531

Contents lists available at ScienceDirect

Physics Letters B

journal homepage: www.elsevier.com/locate/physletb

Search for nonresonant Higgs boson pair production in final state with two bottom quarks and two tau leptons in proton-proton collisions at $\sqrt{s} = 13$ TeV

The CMS Collaboration *

CERN, Geneva, Switzerland

ARTICLE INFO

Article history:
Received 19 June 2022
Received in revised form 11 September 2022
Accepted 18 October 2022
Available online 19 May 2023
Editor: M. Doser

Keywords:
CMS
Higgs
HH
Bbtautau
Self-coupling
VBF

ABSTRACT

A search for the nonresonant production of Higgs boson pairs (HH) via gluon-gluon and vector boson fusion processes in final states with two bottom quarks and two tau leptons is presented. The search uses data from proton-proton collisions at a center-of-mass energy of $\sqrt{s} = 13$ TeV recorded with the CMS detector at the LHC, corresponding to an integrated luminosity of 138 fb^{-1}. Events in which at least one tau lepton decays hadronically are considered and multiple machine learning techniques are used to identify and extract the signal. The data are found to be consistent, within uncertainties, with the standard model (SM) predictions. Upper limits on the HH production cross section are set to constrain the parameter space for anomalous Higgs boson couplings. The observed (expected) upper limit at 95% confidence level corresponds to 3.3 (5.2) times the SM prediction for the inclusive HH cross section and to 124 (154) times the SM prediction for the vector boson fusion HH cross section. At 95% confidence level, the Higgs field self-coupling is constrained to be within −1.7 and 8.7 times the SM expectation, and the coupling of two Higgs bosons to two vector bosons is constrained to be within −0.4 and 2.6 times the SM expectation.

1. Introduction

The discovery of the Higgs boson (H) by the ATLAS and CMS Collaborations [1–3] was a major step towards improving the understanding of the mechanism of electroweak symmetry breaking. With the value of the H mass (m_{H}) experimentally measured by the CMS Collaboration to be 125.38 ± 0.14 GeV [4], the structure of the Higgs scalar field potential and the strength of the H self-coupling are precisely predicted in the standard model (SM). While the measured properties are so far consistent with the SM [5], determining the H self-coupling provides an independent test of the SM and is fundamental to probe experimentally the shape of the scalar potential that is at the base of the electroweak symmetry breaking mechanism.

The trilinear self-coupling of the Higgs boson (λ_{HHH}) can be extracted from the measurement of the Higgs boson pair (HH) production cross section. In the SM, the HH production occurs for proton-proton (pp) collisions at the LHC mainly via gluon-gluon fusion (ggF), involving either couplings to a loop of virtual fermions, or the λ_{HHH} coupling itself. The leading-order (LO) gg → HH Feynman diagrams shown in Fig. 1 have approximately the same amplitude but interfere destructively, therefore reducing the production cross section. The SM prediction for the HH production cross section, computed at the next-to-next-to-LO (NNLO) precision for a center-of-mass energy of $\sqrt{s} = 13$ TeV, is $\sigma_{\text{ggF}}^{\text{HH}} = 31.05^{+6\%}_{-23\%}$ (scale + m_{t}) ± 3% (PDF + α_{S}) fb for an m_{H} of 125 GeV [6,7], where PDF is the parton distribution function, α_{S} is the strong coupling constant and m_{t} is the mass of the top quark.

Among the other HH production modes, vector boson fusion (VBF) is of particular interest as it is the second-largest contribution to HH production and it gives access to the coupling between one or two H and two vector bosons. Despite its small production cross section, $\sigma_{\text{VBF}}^{\text{HH}} = 1.726^{+0.03\%}_{-0.04\%}$ (scale) ± 2.1% (PDF + α_{S}) fb at next-to-NNLO precision for $\sqrt{s} = 13$ TeV [8], the distinctive VBF topology provides a useful handle to identify signal events, thanks to its two forward jets being well separated in pseudorapidity (η) and with a large invariant mass. The LO Feynman diagrams for VBF HH production are shown in Fig. 2.

Beyond SM physics effects in the nonresonant case can appear via anomalous couplings of the H or via new particles that contribute to the virtual quantum loops in Fig. 1. The experimental

* *E-mail address:* cms-publication-committee-chair@cern.ch.

https://doi.org/10.1016/j.physletb.2022.137531

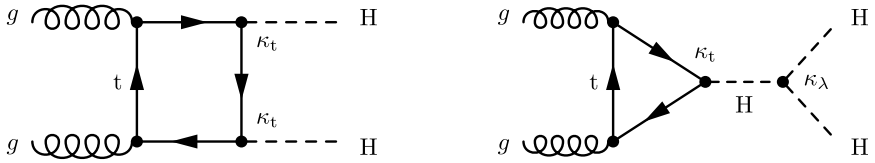

Fig. 1. Feynman diagrams contributing to HH production via gluon-gluon fusion in the SM at leading order. The different H interactions are labelled by the coupling modifiers κ.

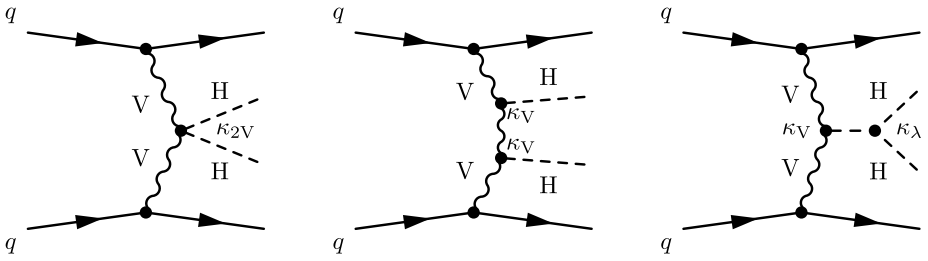

Fig. 2. Feynman diagrams contributing to Higgs boson pair production via vector boson fusion in the SM at leading order. The different H interactions are labelled with the coupling modifiers κ.

signature would be a modification of the HH production cross section and of the event kinematical properties [9].

The variation of λ_{HHH} with respect to the SM prediction is parameterized by the coupling modifier $\kappa_\lambda = \lambda_{HHH}/\lambda^{SM}_{HHH}$, which affects both the ggF and the VBF production mechanisms. Similarly, the variations of the coupling of the H to the top quark are parameterized as κ_t, while those of the couplings involved in the VBF production are parameterized as κ_V (V VH coupling) and κ_{2V} (VVHH coupling).

In this paper, we present a search for HH production in pp collisions at $\sqrt{s} = 13\,\text{TeV}$, investigating both the ggF and the VBF production mechanisms. The final state where one H decays to $b\bar{b}$ and the other decays to $\tau^+\tau^-$ (for simplicity $HH \to bb\tau\tau$), characterized by a decay branching fraction of 7.3% for $m_H = 125\,\text{GeV}$, is studied. The sizable branching fraction, combined with the precise tau lepton identification algorithms developed within the CMS Collaboration (DeepTau [10]), makes this final state one of the most sensitive to HH production. We consider three decay modes of the $\tau\tau$ system: $\tau_\mu\tau_h$, $\tau_e\tau_h$, and $\tau_h\tau_h$, where τ_μ, τ_e, and τ_h correspond, respectively, to the decay of a tau lepton into a muon, an electron, or hadrons, with the associated neutrinos. These account for 87.6% of the full $\tau\tau$ decay modes. Quantum chromodynamics (QCD) multijet and $Z/\gamma^* \to \ell\ell$ events represent the dominant background in the fully hadronic channel, while in the semileptonic channels $t\bar{t}$ events represent the largest contamination. The data used in this analysis correspond to an integrated luminosity of $138\,\text{fb}^{-1}$ collected during 2016–2018 by the CMS experiment.

The search described in this paper improves on the previous $HH \to bb\tau\tau$ results from the CMS and ATLAS Collaborations [11,12] by making use of a larger data sample, an improved trigger strategy, and the introduction of several newly developed neural networks that identify the b jets from the H decay, categorize the events, and perform signal extraction. Moreover, this analysis builds up on CMS-wide innovations such as the new DeepTau [10] and DeepJet [13] algorithms. All these factors lead to achieving particularly stringent results on the HH production cross sections.

Tabulated results are provided in the HEPData record for this analysis [14].

2. The CMS detector

The CMS detector is a multipurpose apparatus optimized to study high-transverse-momentum (p_T) physics processes in pp collisions. The central feature of the CMS detector is a superconducting solenoid, providing a magnetic field of 3.8 T. Within the solenoid volume are a silicon pixel and strip tracker that cover a region of $|\eta| < 2.5$, a lead tungstate crystal electromagnetic calorimeter (ECAL), and a brass and scintillator hadron calorimeter (HCAL), each composed of a barrel and two endcap sections that cover $|\eta| < 3$. Forward calorimeters extend the η coverage, provided by the barrel and endcap detectors, to $|\eta| < 5$. Muons are detected in gas-ionization chambers embedded in the steel flux-return yoke outside the solenoid and covering an angle $|\eta| < 2.4$. Events of interest are selected using a two-tiered trigger system. The first level (L1), composed of custom hardware processors, uses information from the calorimeters and muon detectors to select events at a rate of around 100 kHz within a fixed latency of about $4\,\mu s$ [15]. The second level, known as the high-level trigger, consists of a farm of processors running a version of the full event reconstruction software optimized for fast processing, and reduces the event rate to around 1 kHz before data storage [16].

A more detailed description of the CMS detector, together with a definition of the coordinate system used and the relevant kinematic variables, can be found in Ref. [17].

3. Data and simulated samples

The data used in this analysis correspond to an integrated luminosity of 36.3, 41.5, and $59.7\,\text{fb}^{-1}$, for the 2016, 2017, and 2018 data-taking periods, respectively [18–20].

Simulated samples of nonresonant HH production via ggF are generated at LO precision with MadGraph5_aMC@NLO v2.4.2 [21] and at next-to-LO (NLO) precision with POWHEG v2.0 [22–24]. The former samples are used for training the machine learning algorithms implemented in this analysis, while the latter are used for the signal extraction: in order to model any arbitrary κ_λ value, the expected distributions of signal events at three support points ($\kappa_\lambda = \{1.00, 2.45, 5.00\}$) are scaled by functions of the target value of κ_λ, defined according to the known dependence of the ggF HH cross section [25], summed together, and then normalized to the corresponding NNLO cross section [6]. Simulated samples of nonresonant HH production via VBF are generated at LO precision with MadGraph5_aMC@NLO v2.3.2.2 (v2.6.0) for 2016 (2017–2018) and a similar procedure for modelling any κ_{2V} value is applied as in the ggF case.

Backgrounds arising from $Z/\gamma^* \to \ell\ell$ production and W boson production in association with jets are simulated with MadGraph5_aMC@NLO at LO with MLM merging [26]; the single top

quark, single H, and $t\bar{t}$ backgrounds are simulated at NLO precision with POWHEG v2.0; backgrounds from diboson (WW, ZZ, and WZ) and triboson (ZZZ, ZZW, ZWW, and WWW) production are simulated at NLO precision with MADGRAPH5_aMC@NLO, both with and without FxFx merging [27], and POWHEG, depending on the process; production of $t\bar{t}$ pairs in association with a single boson or a pair of vectors bosons are simulated with MADGRAPH5_aMC@NLO, both with and without FxFx merging, depending on the process. For the simulation of backgrounds using MADGRAPH5_aMC@NLO, different versions of the generator are used (2.2.2, 2.3.2.2, 2.3.3, and 2.4.2), depending on the process and year. LO samples use the MLM merging allowing up to four extra partons in the matrix element, while for NLO samples generated with the FxFx merging only one extra parton is allowed.

For both signal and background events, multiparton, parton shower, and hadronization effects are simulated with PYTHIA v8.226 for 2016 and PYTHIA v8.230 for 2017–2018 [28]. For 2016, the CUETP8M1 [29] tune is used for all the samples, except for the single top and $t\bar{t}$ samples, which rely on the CP5 [30] tune; for 2017–2018, the CP5 tune is used throughout all samples. The utilized parton distributions functions are the NNPDF 3.0 [31] set for 2016 data sets and the NNPDF 3.1 [32] set for 2017–2018 data sets. For all simulated samples, the CMS detector response is modeled with GEANT4 [33]. Additional collisions within the same or nearby bunch crossings (pileup) are simulated and added to the hard-scattering process for all samples. Events are then reweighted to match the pileup profile observed in data.

4. Event reconstruction and selection

The event reconstruction is based on the particle-flow (PF) algorithm [34], which aims to reconstruct and identify each individual particle (PF candidate) in an event, with an optimized combination of information from the various elements of the CMS detector. PF candidates are classified as electrons, muons, photons, and charged or neutral hadrons. An important portion of the $bb\tau\tau$ final state is reconstructed and identified through the combination of PF objects, such as the jets originating from b quarks, the τ_h candidates, and the missing transverse momentum vector $\vec{p}_T^{\,miss}$, computed as the negative vector p_T sum of all the PF candidates in an event. The magnitude of the $\vec{p}_T^{\,miss}$ vector is denoted as p_T^{miss} [35]. The primary vertex (PV) is taken to be the vertex corresponding to the hardest scattering in the event, evaluated using tracking information alone, as described in Section 9.4.1 of Ref. [36].

The electron momentum is estimated by combining the energy measurement in the ECAL with the momentum measurement in the tracker. The momentum resolution for electrons with $p_T \approx 45$ GeV from $Z \to ee$ decays ranges from 1.6 to 5.0%. It is generally better in the barrel region than in the endcaps, and also depends on the bremsstrahlung energy emitted by the electron as it traverses the material in front of the ECAL [37,38]. Electron identification (ID) is based on a boosted decision tree (BDT) that combines purely-ECAL, purely-tracker, and ECAL-plus-tracker observables, including the isolation of the electron. The "tight" working point of this discriminator, characterized by an 80% efficiency, is employed in the analysis [37].

Muons are measured in the range $|\eta| < 2.4$, with detection planes made using three technologies: drift tubes, cathode strip chambers, and resistive plate chambers. The single muon trigger efficiency exceeds 90% over the full η range, and the efficiency to reconstruct and identify muons is greater than 96%. Matching muons to tracks measured in the silicon tracker results in a relative p_T resolution, for muons with p_T up to 100 GeV, of 1% in the barrel and 3% in the endcaps. The p_T resolution in the barrel is better than 7% for muons with p_T up to 1 TeV [39]. The isolation of muon candidates (I^{ℓ}_{rel}) is defined as the p_T sum of PF candidates inside a $\Delta R = \sqrt{(\Delta\eta)^2 + (\Delta\phi)^2} < 0.4$ cone around the muon relative to the p_T^{ℓ} of the muon (where ϕ is the azimuthal angle in radians):

$$\frac{\sum p_T^{\text{charged}} + \max\left[0, \sum p_T^{\text{neutral-had}} + \sum p_T^{\gamma} - \frac{1}{2}\sum p_T^{\text{PU}}\right]}{p_T^{\ell}}, \qquad (1)$$

where $\sum p_T^{\text{charged}}$, $\sum p_T^{\text{neutral-had}}$, and $\sum p_T^{\gamma}$ are the scalar sums of the transverse momenta of charged hadrons originating from the PV, neutral hadrons and photons, respectively, and $\sum p_T^{\text{PU}}$ is the sum of transverse momenta of charged hadrons not originating from the PV. In this analysis, the signal muon candidates are required to have $I^{\ell}_{rel} < 0.15$ and to pass the "tight" identification criteria described in Ref. [39]. The combined identification and isolation efficiency varies between 90 and 99% in the p_T range 20–200 GeV.

Hadronic decays of τ leptons are reconstructed using the "hadrons-plus-strips" algorithm [40–42], which classifies individual hadronic decay modes of the τ by combining charged hadrons from the PF reconstruction with neutral pions. The latter are reconstructed by clustering electrons and photons into rectangular strips, which are narrow in η but wide in the ϕ dimension. The spread in ϕ accounts for photons originating from neutral pion decays, which convert into electron-positron pairs while traversing the silicon tracker. These particles are bent in opposite directions in ϕ by the magnetic field, and may further emit bremsstrahlung photons before reaching the ECAL. The decay modes considered in this analysis produce one charged pion or kaon plus zero, one or two neutral pions, or three charged pions or kaons plus zero or one neutral pion. The DEEPTAU algorithm identifies τ_h objects using a convolutional neural network combining information from high-level tau lepton observables together with low-level features obtained from the silicon tracker, the ECAL and HCAL, and the muon detectors for all the PF candidates, electrons, and muons that are reconstructed inside the tau lepton isolation cone ($\Delta R < 0.5$). Three different discriminants are employed in order to distinguish τ_h candidates from jets ("DEEPTAUVSJETS"), electrons ("DEEPTAUVSELE") and muons ("DEEPTAUVSMU"). Different working points are used in each analysis channel, as summarized in Table 1.

Jets are reconstructed offline from PF candidates, clustered using the anti-k_T algorithm [43,44] with distance parameters of 0.4 and 0.8, respectively, denoted as "AK4" and "AK8" jets. The constituents of the AK8 jets are reclustered using the Cambridge–Aachen algorithm [45,46]; the "modified mass drop tagger" algorithm [47,48], also known as the "soft-drop" algorithm, is applied to remove soft, wide-angle radiation from the jet. The jet momentum is determined as the vectorial sum of all particle momenta in the jet, and is found from simulation to be, on average, within 5–10% of the true momentum over the entire p_T spectrum and detector acceptance. Pileup collisions can give rise to jets not coming from the hard-scattering process (pileup jets) or contribute additional tracks and calorimetric energy depositions, increasing the apparent jet momentum. For AK4 jets, to mitigate this effect, tracks identified to be originating from pileup vertices are discarded and an offset is applied to correct for remaining contributions [49]. For AK8 jets, the pileup-per-particle identification algorithm [50] is used to mitigate the effect of pileup at the reconstructed particle level, making use of local shape information, event pileup properties, and tracking information. Jet energy corrections are derived from simulation studies so that the average measured energy of jets becomes identical to that of particle-level jets. In situ measurements of the momentum balance in dijet, γ + jets, Z + jets, and multijet events are used to determine any residual differences between the jet energy scale in data and in simulation, and appropriate corrections are applied [51,52]. Jets originating from b

Table 1
Summary of selections applied to the $\tau\tau$ candidate pair. Trigger thresholds in parentheses refer to the 2017–2018 data-taking period when different from 2016.

Online p_T trigger thresholds	single-e: $p_T > 25$ (32) GeV cross-e: electron $p_T > 24$ GeV, τ_h $p_T > 30$ GeV single-μ: $p_T > 22$ (24) GeV cross-μ: muon $p_T > 19$ (20) GeV, τ_h $p_T > 20$ (27) GeV ditau: $p_T > 35$ GeV, ditau VBF: $p_T > 20$ GeV
Offline p_T thresholds	online threshold +1 GeV (electrons and muons) online threshold +5 GeV (τ_h candidates)
η thresholds	electrons and muons: $\lvert\eta\rvert < 2.1$ tau: $\lvert\eta\rvert < 2.1$ (2.3) for ditau and cross (single) triggers
Lepton ID and isolation	tight electron BDT ID + isolation tight muon ID and isolation
τ_h ID ($\tau_e\tau_h$, $\tau_\mu\tau_h$ channels)	medium DeepTauVsJet tight DeepTauVsMu very-loose DeepTauVsEle
τ_h ID ($\tau_h\tau_h$ channel)	medium DeepTauVsJet very-loose DeepTauVsMu very-very-loose DeepTauVsEle
Distance to PV	$\lvert d_{xy}\rvert < 0.045$ cm (electrons and muons only) $\lvert d_z\rvert < 0.2$ cm
Pair selections	opposite-sign, $\Delta R > 0.5$

quarks are identified using the DeepJet algorithm [13], a deep neural network combining secondary vertex properties, track-based variables, and PF jet constituents (neutral- and charged-particle candidates). Different thresholds applied to the output of the DeepJet algorithm result in working points characterized by their b tagging accuracy; in this analysis the "loose" and "medium" working points are used, corresponding to an efficiency (misidentification rate for light-flavor and gluon jets) of 94 (10)% and 84 (1)%, respectively [13].

As mentioned in the introduction, this analysis considers three decay modes of the $\tau\tau$ system: $\tau_\mu\tau_h$, $\tau_e\tau_h$, and $\tau_h\tau_h$. Different trigger strategies are employed for each of these channels. In the semileptonic ones, single-lepton and cross-lepton triggers are used. The former requires the presence of an isolated electron or muon only, while the latter also requires an additional hadronically decaying tau lepton. The use of cross-triggers represents the main change in the trigger strategy with respect to the result previously published on 2016 data [11] and improves the analysis sensitivity, allowing the p_T threshold on electrons and muons to be lowered, as described in Table 1. In the $\tau_h\tau_h$ channel, triggers requiring the presence of a pair of hadronically decaying τ leptons with $p_T > 35$ GeV are employed. A VBF ditau trigger was introduced in 2017 to extend the analysis phase space, targetting events containing two hadronically decaying τ leptons with $p_T > 20$ GeV and two jets, one with $p_T > 115$ GeV and the other with $p_T > 45$ GeV. The online trigger thresholds for each electron, muon or tau lepton are reported in Table 1. Compared to the online selection, the offline thresholds are increased by 1 GeV for electrons and muons and by 5 GeV for τ_h candidates: this is done to assure that the trigger efficiency reaches its plateau value.

Events are classified in three different $\tau\tau$ decay channels based on the information from the τ lepton candidates reconstructed offline. Selected signal events are required to have at least one τ_h candidate. An event is classified as $\tau_\mu\tau_h$ if a muon passing the selections detailed in Table 1 is found, otherwise it is classified as $\tau_e\tau_h$ if an electron passing the selections is found: if neither a muon nor an electron is found, the event is classified as $\tau_h\tau_h$ if a second τ_h is present. In the $\tau_h\tau_h$ channel, if not stated otherwise, the former τ_h refers to the more isolated one.

Each reconstructed electron, muon, or tau lepton candidate is required to have a distance between the track of the candidate and the PV in the transverse and longitudinal planes satisfying $\lvert d_{xy}\rvert < 0.045$ cm (electrons and muons only) and $\lvert d_z\rvert < 0.2$ cm. The two objects forming a pair must have opposite charge and be separated by $\Delta R > 0.5$. To reduce $Z/\gamma^* \to \ell\ell$ contamination, a third-lepton veto is applied, by discarding events where additional electrons or muons are present.

Finally, events selected with the above described criteria are required to have at least two additional AK4 jets with $p_T > 20$ GeV, $\lvert\eta\rvert < 2.4$, and $\Delta R(j, \ell) > 0.5$, where ℓ represents each of the two leptons forming the $\tau\tau$ candidate pair. Studies on the previous published bb$\tau\tau$ result [11] highlighted the selection of the $H \to bb$ candidate as being one of the least efficients. A new b jet assignment algorithm (referred to as HH-bTag) has therefore been developed, based on a neural network architecture. The input features of the network include the b jets and $H \to \tau\tau$ system kinematic variables, the DeepJet score of the b jet candidates, and their angular separation with respect to the $H \to \tau\tau$ candidate. For each event, all possible b jet candidates are assigned a score by the HH-btag algorithm; the two jets with the highest scores are taken as those originating from the decay of the H. Two additional jets are looked for amongst all the remaining jets with $p_T > 30$ GeV and $\lvert\eta\rvert < 4.7$. Among all the additional jets in the event, all possible pairs are built and that with the highest invariant mass (m_{jj}) is chosen as the VBF candidate pair. In case the event was selected by the VBF ditau trigger, and not by the other ditau triggers, due to the lower p_T thresholds on τ_h candidates, three additional requirements are then made: $m_{jj} > 800$ GeV, $p_T > 140$ GeV and 60 GeV for the leading and subleading VBF jet candidates.

The selections on leptons and jets described in this section and in Table 1 lead to a final efficiency and acceptance product of 5.5 (3.4)% for the ggF (VBF) SM signal events.

5. Event categorization and discriminating variables

Events selected as described in Section 4 are classified in eight mutually exclusive categories, in order to maximize the sensitivity to both the ggF and VBF HH searches.

In order to categorize signal events produced through the VBF mechanism, a selection (denoted "VBF inclusive") is introduced by requiring that two VBF jet candidates, as described in Section 4, can be identified in the event and that they further pass two

requirements (jointly referred to as the "VBF tag") designed to reduce the background contamination: $m_{jj} > 500\,\text{GeV}$ and a separation in pseudorapidity ($\Delta\eta$) between the two VBF jet candidates larger than 3. Because of the ggF signal contamination in the VBF inclusive selection, in order to enhance the analysis sensitivity, a multiclassification approach is introduced that allows to create two additional signal categories (*classVBF* for the HH VBF events and *classGGF* for the ggF contribution), as well as three background-enriched ones (*classttH* for $t\bar{t}H$ events, *classTT* for the $t\bar{t}$ contamination, and *classDY* for the $Z/\gamma^* \to \ell\ell$ contribution), used to constrain the systematic uncertainties affecting these processes. Each event is assigned to the category for which it has the highest multiclassifier score. The score represents the probability of originating from the specific process denoted by the category name.

Events without two VBF jet candidates identified, or with two VBF jet candidates identified but not passing the VBF tag selection, are classified exploiting the differences in Lorentz boost regimes of $b\bar{b}$ production in order to increase the analysis sensitivity. If the two b jets have $\Delta R(b, b) > 0.8$, jets are reconstructed as separated AK4 jets; on the other hand, if they have $\Delta R(b, b) < 0.8$ then they are merged and reconstructed as a single AK8 jet. In the first case, the jets are referred to as "resolved", in the latter case as "boosted". To be categorized as boosted, events are required to have a minimal AK8 jet mass of 30 GeV, a distance between the two subjets and the previously selected AK4 jets of $\Delta R < 0.4$, and both the subjets must pass the loose b tagging working point. All events not satisfying these requirements are categorized as resolved. In addition, resolved events are split into two categories depending on the b tag multiplicity: events where only one jet passes the medium b tagging working point (*res1b*), and events where both jets pass this working point (*res2b*).

After object selection and event categorization, the kinematic information in the events is used to introduce additional requirements on the invariant masses of the b jet candidates (m_{bb}) and the tau lepton candidates ($m_{\tau\tau}$): the latter is reconstructed using the SVfit algorithm [53], a dynamic likelihood technique combining the kinematical properties of the two visible lepton candidates and the p_T^{miss} in the event. Events satisfying the invariant mass requirements constitute the signal region (SR) of the analysis. For the resolved categories the selection is:

$$\frac{(m_{\tau\tau} - 129\,\text{GeV})^2}{(53\,\text{GeV})^2} + \frac{(m_{bb} - 169\,\text{GeV})^2}{(145\,\text{GeV})^2} < 1, \quad (2)$$

while for the *boosted* category, because of its different kinematical properties, the selection is:

$$\frac{(m_{\tau\tau} - 128\,\text{GeV})^2}{(60\,\text{GeV})^2} + \frac{(m_{bb} - 159\,\text{GeV})^2}{(94\,\text{GeV})^2} < 1. \quad (3)$$

No invariant mass requirement is applied to the VBF multicategories.

In Eqs. (2) and (3), the mass offsets (numerator) and resolutions (denominator) are chosen using a random search that minimizes the background acceptance for a signal efficiency larger than 90%. Contrary to what was done in Ref. [11], the purpose of the invariant mass selection is no longer to maximize the signal significance, but rather to remove significantly outlying background events in regions where no signal is expected, while the discrimination of HH events from the background is left to a specifically designed neural network, as described in the next paragraph.

The eight orthogonal categories (*res2b*, *res1b*, *boosted*, *classVBF*, *classGGF*, *classttH*, *classTT* and *classDY*) obtained are used for the signal extraction via a deep neural network developed to identify $HH \to bb\tau\tau$ events. In the following, this discriminating algorithm will be referred to simply as DNN. A single training is performed with events from all years, channels and categories, obtained from the simulated background and the SM HH signal samples as described in Section 3. The scope of the training is to classify events as originating either from signal or background processes by assigning them a single prediction. Predictions closer to zero indicate "background-like" events, while predictions closer to one indicate "signal-like" events. The final DNN distributions used in the signal extraction fit are obtained by inferring predictions of the trained network separately in each of the eight orthogonal categories, split by channel and year.

The DNN is composed of two discriminators, each consisting of ten neural networks trained via ten-fold stratified cross-validation of the training set. The architecture of the networks is the same as the optimal architecture developed in Ref. [54], with the addition of increased overfitting supervision [55,56]. The approach used to train the DNN [57–60] follows that used in the CMS HH High-Luminosity LHC projection analysis for the $bb\tau\tau$ final state [61,62]. In this approach, the simulated events are split evenly into two subsets and each discriminator of the DNN is trained on a different subset. At the inference stage, the discriminators are used in the subset of events on which they were not trained. Thus, all of the simulated events are used for inference, reducing the associated statistical uncertainty on the sample density distributions, while not being subject to a systematic bias in the predictions that would otherwise arise if the discriminators were applied to events on which they were actually trained. It should be noted that this approach does not provide an explicit validation sample, and does therefore not permit any fine-tuning of hyper-parameters without the risk of biasing the model. Nevertheless, the lack of tuning is not expected to significantly impair the performance of the DNN [54]. A total of 26 features (selected from a starting pool of over 100) are used as an input to the DNN. Besides the categorical features, such as the year of data taking, the $\tau\tau$ decay mode, and the number of VBF jet candidates, among the most important features are the DeepJet scores of the b jets, binned in working points, the invariant masses of the HH, $\tau\tau$, and bb systems, and several kinematic variables, such as visible momenta and distances in the $\eta - \phi$-plane between reconstructed particles, describing the spatial distribution of the physics objects in the event.

6. Background modeling

The main background sources contaminating the SR are $t\bar{t}$ production, $Z/\gamma^* \to \ell\ell$ production, and QCD multijet events; all three are modeled using specific approaches. The productions of single top, single H, W boson in association with jets, diboson, triboson, and $t\bar{t}$ pairs in association with a single boson or a pair of vectors bosons are instead estimated from simulation, as described in Section 3. For all backgrounds, except multijet, both events with real hadronically decaying tau leptons and with lepton or quark or gluon jets misidentified as τ_h candidates are taken from simulation. The fraction of misidentified τ_h candidates in the dominant background ($t\bar{t}$) is lower than 20% in the analysis SR. No specific correction is applied to compensate for potential differences between simulation and data for fake τ_h candidates, but a systematic uncertainty is added to the fit model as described in Section 7.

The $t\bar{t}$ background contribution is modeled relying on simulation. The normalization of the background shows a disagreement with respect to the observed data, thus a correction scale factor (*ttSF*) is fitted from a $t\bar{t}$-enriched control region (CR). Three CRs are defined, one for each year, to contain $\tau_e\tau_h$, $\tau_\mu\tau_h$, and $\tau_h\tau_h$ events that satisfy the *res2b* selections outlined in Section 5 and pass a mass requirement obtained by inverting, among the resolved categories, the one defined in Eq. (2). The contamination from other backgrounds in the $t\bar{t}$-enriched CR is less than 9% for all three years. The *ttSF*s resulting from the fit are 0.908, 0.988, and 0.966

for 2016, 2017, and 2018, respectively, with an uncertainty, also coming from the fit, that ranges between 0.6 and 0.9%.

The $Z/\gamma^* \to \ell\ell$ background contribution is modeled relying on simulation. Scale factors for the simulation normalization are taken from 18 CRs containing events with two isolated muons compatible with the $Z \to \mu\mu$ decay. The same jet selection criteria as in the SR are applied in the CRs. The CRs are defined as follows: the data are first split into three CRs based on the number of b-tagged jets (0, 1, or 2); each CR so obtained is further split into six CRs based on the p_T of the reconstructed Z candidate. Simulated events are split, obtaining 18 templates based on the number of b partons at the generator level and the p_T of the generator-level Z boson; one additional template, combining all other backgrounds, is also considered. The scale factors are obtained performing a simultaneous fit of the di-muon mass in the CRs using the 19 templates, where their normalizations are kept floating.

The multijet background contribution is determined from data in jet-enriched regions where the tau lepton pair requirements are inverted. Two different shapes are obtained in regions where either the pair charge or the τ_h isolation requirement is inverted (in the $\tau_h\tau_h$ final state, only the isolation requirement on the lowest p_T τ_h candidate is inverted) and all the other selections are applied as in the SR. The final multijet background template is then defined as the mean of these two shapes. The yield is obtained as the product of the yields in the two regions defined above divided by the yield obtained in the region where both the charge and isolation requirements are inverted. The contributions of other backgrounds, based on predictions as outlined above, are subtracted in all these regions.

A comparison of data and simulation prediction, corrected as described in this Section, for three of the most important input features of the DNN described in Section 5 is shown in Fig. 3.

7. Systematic uncertainties

In this analysis, we include various sources of systematic uncertainty that originate from a limited knowledge of the background and signal processes, discrepancies between simulation and data, and imperfect knowledge of the detector response. They are categorized as "normalization" and "shape" uncertainties: while the first affect only the total event yield of the processes, the latter affect also the distribution of the events. The uncertainties described in this Section are introduced as nuisance parameters in the maximum likelihood fit described in Section 8, with log-normal (Gaussian) priors for normalization (shape) uncertainties.

The following normalization uncertainties are considered.

- Different sources of uncertainty in the integrated luminosity measurement are considered and treated as correlated. Their values are obtained from dedicated Van-der-Meer scans and the stability of detector response during data taking. The integrated luminosities for the 2016, 2017, and 2018 data-taking years have 1.2–2.5% individual uncertainties [18–20], while the overall uncertainty for the 2016–2018 period is 1.6%. These uncertainties are applied only to the signals and to background processes estimated from simulation. Since the normalizations of the $t\bar{t}$, $Z/\gamma^* \to \ell\ell$, and multijet backgrounds are obtained from data, they are not subject to the integrated luminosity uncertainties.
- Electron and muon reconstruction, isolation, and identification uncertainties are determined from the simulation-to-data scale factors; a value of 1% for both electrons and muons is obtained [37,39]. An additional uncertainty of 3 (15)% for tau leptons with $p_T < 100$ GeV (> 100 GeV) is added in the $\tau_h\tau_h$ channel [10].
- During the 2016–2017 data taking, a gradual shift in the timing of the inputs of the ECAL L1 trigger in the region at $|\eta| > 2.0$ caused a trigger inefficiency. For events containing an electron (a jet) with $p_T > 50$ (100) GeV, in the region $2.5 < |\eta| < 3.0$ the efficiency loss is approximately 10–20%, depending on p_T, η, and time. Correction factors were computed from data and applied to the acceptance evaluated by simulation. An uncertainty of 2% is assigned to this effect.
- The uncertainty in the pileup reweighting technique is estimated by varying the values of the applied pileup weights by their uncertainty. The resulting systematic uncertainty is estimated to have a value of 1% and it is correlated among all channels and categories in each year.
- The normalization of the $t\bar{t}$ background is taken from a fit to a CR per year, as described in Section 6. The uncertainty in the scale factors obtained in these CRs is purely statistical and is always below 1%.
- The normalization of the $Z/\gamma^* \to \ell\ell$ background is taken from a fit to 18 CRs per year, as described in Section 6. The uncertainties in the scale factors obtained in these CRs are propagated to the SR taking into account their correlation and range from 0.1 to 60% depending on the year and CR considered.
- The multijet background contribution is determined from data in jet-enriched regions, as described in Section 6. Two normalization uncertainties are derived in order to take into account the event yields statistical fluctuations in these CRs and their dependence on the τ_h isolation requirement used to define them.
- The uncertainties in the normalizations of the backgrounds modeled relying solely on the simulated events range from 2 to 10%.
- The theoretical uncertainty in the cross section of HH production: via ggF: $^{+6\%}_{-23\%}$ (scale + m_t), $\pm 3\%$ (PDF + α_S) fb [6]; and via VBF: $^{+0.03}_{-0.04}\%$ (scale) and $\pm 2.1\%$ (PDF + α_S) [8]. These uncertainties are only considered when upper limits are quoted with respect to the SM and for the likelihood scans, they are not included for the upper limits on the cross section.
- The theoretical uncertainty in the H branching fractions [63] amount: for the decay to $b\bar{b}$, to $\pm 0.65\%$ (theory), $^{+0.72}_{-0.74}\%$ (m_q), $^{+0.78}_{-0.80}\%$ (α_S), where m_q is the quark mass; and for the decay to tau leptons to $^{+1.16}_{-1.17}\%$ (theory), $^{+0.98}_{-0.99}\%$ (m_q), 0.62% (α_S).
- The uncertainty in the modeling of the VBF signal in PYTHIA8 is estimated through samples generated setting the dipole recoil option, which affects the initial-state parton showers, to ON [64]. The ratio of integrated yields in the dipole recoil ON/OFF samples is taken as the uncertainty: it varies from 10% for largely populated categories such as *classVBF*, to 70% for categories with poor VBF signal contribution, such as *classttH*.

The following shape uncertainties are considered.

- The uncertainty in the measurement of the energy of τ_h leptons [10]. The uncertainties are derived by combining low- and high-p_T measurements in $Z \to \tau\tau$ and in the off-shell $W^* \to \tau\nu$ events. Four different uncertainties are included to take into account the different τ_h decay modes considered in this analysis. When considering the uncertainty for a particular decay mode, the shift is applied only to the τ_h candidates that are reconstructed with that particular decay mode, while all other τ_h candidates are left unchanged.
- Uncertainties related to the calibration of jet energy scale (JES) and resolution (JER). For JES, 11 separate sources of uncertainty are included per year: those appearing in multiple years are treated as fully correlated, while those appearing only in one year are treated as uncorrelated. For JER, alternative tem-

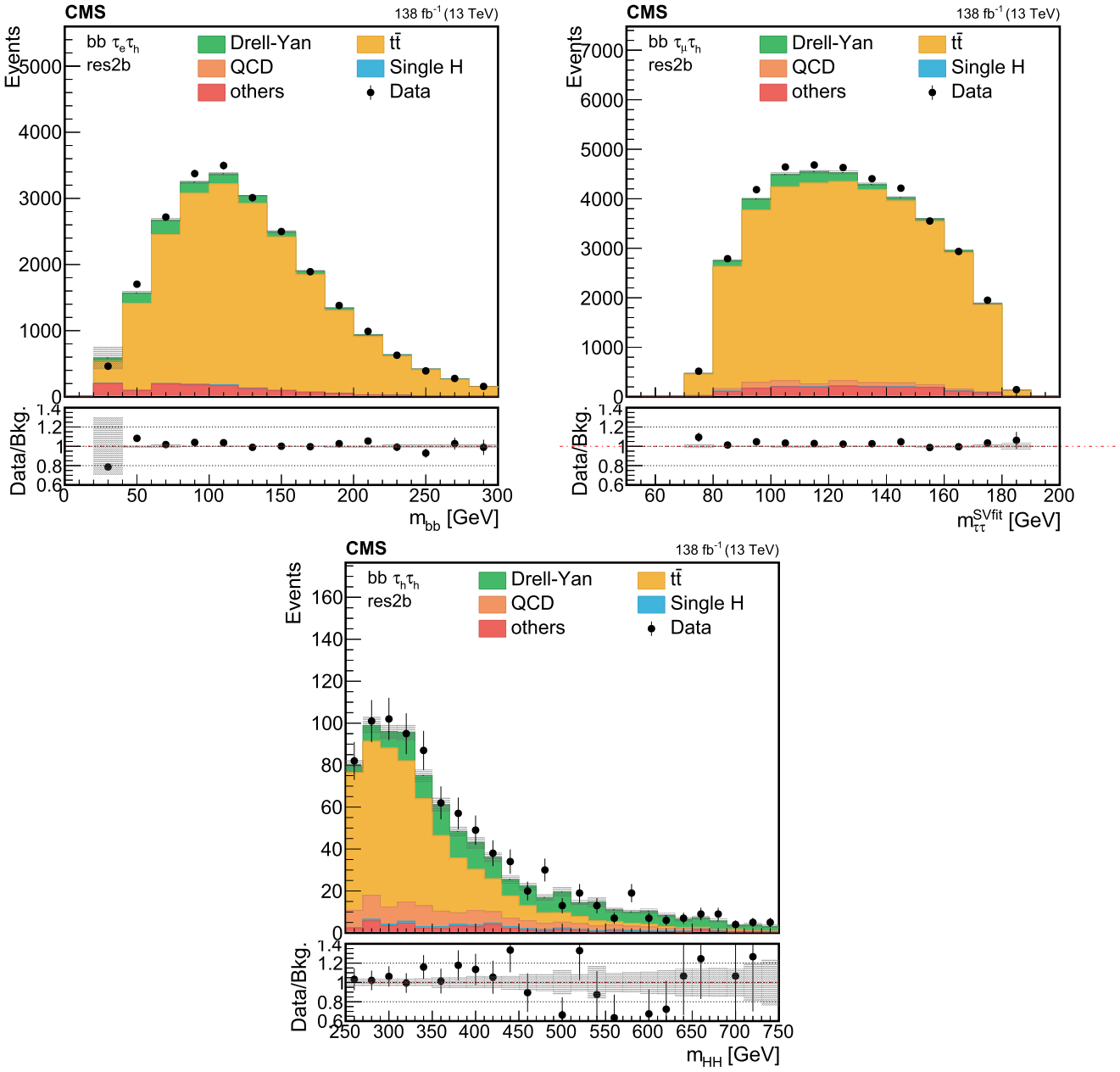

Fig. 3. Distributions of the reconstructed mass of the bb (upper left), ττ (upper right) and HH (lower) pairs in the most sensitive category of the analysis (*res2b*). Events are shown in the $\tau_e\tau_h$ (upper left), $\tau_\mu\tau_h$ (upper right) and $\tau_h\tau_h$ (lower) channels for the full 2016–2018 data set, after the selection on the reconstructed masses of the ττ and bb pairs, as described in Section 5. The shaded band in the plots represents the statistical uncertainty only.

plates are produced by shifting all the jet-related features. These shifts stem from the use of scale factors to smear the energy of simulated jets to match the observed energy resolution in data.

- Separate uncertainties in the energy scale of electrons misidentified as τ_h candidates are provided to take into account two different decay modes, $h^\pm$ and $h^\pm\pi^0$. The uncertainty in the energy scale of muons misidentified as τ_h candidates is 1%, uncorrelated across decay modes.
- The uncertainties arising from the application of the DeepTau identification scale factors are determined using a tag-and-probe procedure as a function of the τ_h candidate p_T. Five uncertainties are computed for the identification of taus against jets and are calculated in p_T bins of the τ_h candidate. All these uncertainties are used in the $\tau_\mu\tau_h$ and $\tau_e\tau_h$ channels, while, since in the $\tau_h\tau_h$ channel both leptons are required to have p_T above a threshold, only the highest p_T bin uncertainty can be applied. Two uncertainties are present in the identification of tau leptons against electrons, one for the barrel and one for the endcap, and are treated as uncorrelated across η bins of the τ_h candidate.
- The shape uncertainty in the multijet contribution is determined from the two alternative templates described in Section 6.
- The uncertainties arising from the misidentification of jets as τ_h candidates are determined from $\tau_\mu\tau_h$ CRs defined inverting the charge sign requirement on the tau leptons and imposing that neither of the b jet candidates pass the "medium" working point of the DeepJet algorithm. Six uncertainties, one for the barrel and one for the endcap for each year, are derived and treated as uncorrelated across years and detector regions.

- Trigger efficiencies and scale factors are measured in a $Z \to \tau\tau \to \mu\nu_\mu\nu_\tau\tau_h\nu_\tau$ enriched region with a tag-and-probe procedure and fitted separately for data and simulation. The uncertainty, determined as a function of the reconstructed τ_h candidate p_T, is taken from the fit. The scale factors are obtained from the data to simulation ratio and their uncertainties are propagated accordingly. Four uncertainties are included to take into account the different τ_h decay modes considered in this analysis. They are applied to the τ_h leg of each channel. Two additional trigger uncertainties are used to cover the cases where the tau lepton decays to an electron or a muon. Finally, one uncertainty is added for the $\tau_h\tau_h$ final state in 2017–2018 to take into account the jet legs scale factors of the VBF trigger.
- The uncertainty in the b-tagging efficiency. This takes into account the contamination from udscg (cb) jets in heavy- (light-) flavor regions, as well as statistical fluctuations in both data and simulation samples used for the computation of the b-tagging efficiency.
- The uncertainties in the pileup jet identification scale factor as functions of p_T and η.

The largest sources of systematic uncertainties come from the imperfect knowledge of the ggF HH production cross section, the statistical fluctuations affecting the multijet background estimation, and the mismodeling of jet and τ leptons identification and reconstruction in simulated samples. The total impact of the systematic uncertainties on the result is approximately 15%.

8. Results

A binned maximum likelihood fit of the DNN prediction to the data is performed in eight categories per channel simultaneously for all three years, for a total of 72 input distributions. The systematic uncertainties described in Section 7 are introduced as nuisance parameters in the likelihood function. Upper limits at 95% confidence level (CL) on the HH production cross section are set using the asymptotic modified frequentist method (asymptotic CL_s) [65–67]. We report here the expected and observed sensitivities for the inclusive (ggF + VBF) HH production cross section as functions of κ_λ, whereas the expected and observed sensitivities for the VBF HH production cross section are reported as functions of κ_{2V}. Coupling modifiers that are not part of the scanning procedure are fixed to unity, which corresponds to the SM prediction.

The binning schemes for the DNN prediction distributions used in the likelihood fit are chosen to minimise the expected upper limit, while keeping the number of bins the smallest possible and ensuring the stability of the fit. The binning schemes start from finely-binned histograms: bins are then merged using Bayesian optimization techniques to find the best performing scheme [68]. To reduce computational complexity, limits are minimized consecutively by combining one category after the other and freezing the binning for all previous histograms. In order to avoid poor modeling of background yield or background uncertainty, each bin is required to contain at least one $t\bar{t}$ and one $Z/\gamma^* \to \ell\ell$ event and to have a weighted background yield larger than 0.03.

The obtained postfit DNN distributions used for the maximum likelihood fit are exemplified in Fig. 4, where the distributions for the two most sensitive categories in the ggF (*res2b*) and VBF (*classVBF*) searches in the $\tau_h\tau_h$ channel in 2018 are shown; the distributions are plotted as a function of the DNN bin number for an easier visualization.

As the total number of distributions is relatively high, we provide distributions that combine the content of bins with equal or similar expected sensitivity in terms of a signal-to-noise ratio, as shown in Fig. 5, separately for the three channels $\tau_e\tau_h$, $\tau_\mu\tau_h$, and $\tau_h\tau_h$, as well as in Fig. 6 for the combination of the full 2016–2018 data set. In each plot, the bins of all input distributions are collected, then ordered according to their exected prefit signal-to-square-root-background ratio, and eventually merged according to a dedicated binning rule. Hence, the right-most bins are most sensitive to the signal, whereas the left-most bins are highly dominated by background contributions.

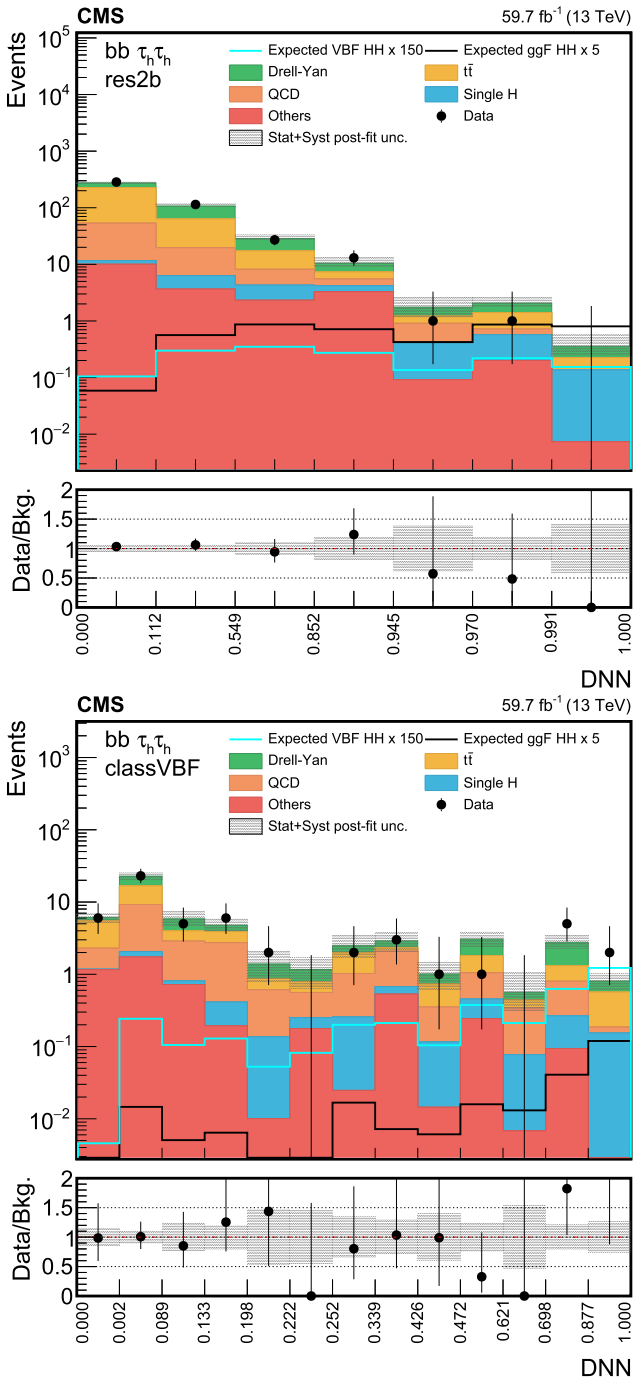

Fig. 4. The postfit DNN distributions in the $\tau_h\tau_h$ channel in 2018 for the most sensitive category in the ggF (upper) and VBF (lower) searches. The shaded band in the plots represents the statistical plus systematic uncertainty. The expected SM distributions for the ggF and VBF HH signals are shown superimposed on the figures.

The expected and observed limits for the ggF plus VBF (inclusive) HH production cross section at the SM point ($\kappa_\lambda = 1$) and those for the VBF only HH production cross section ($\kappa_{2V} = 1$) are

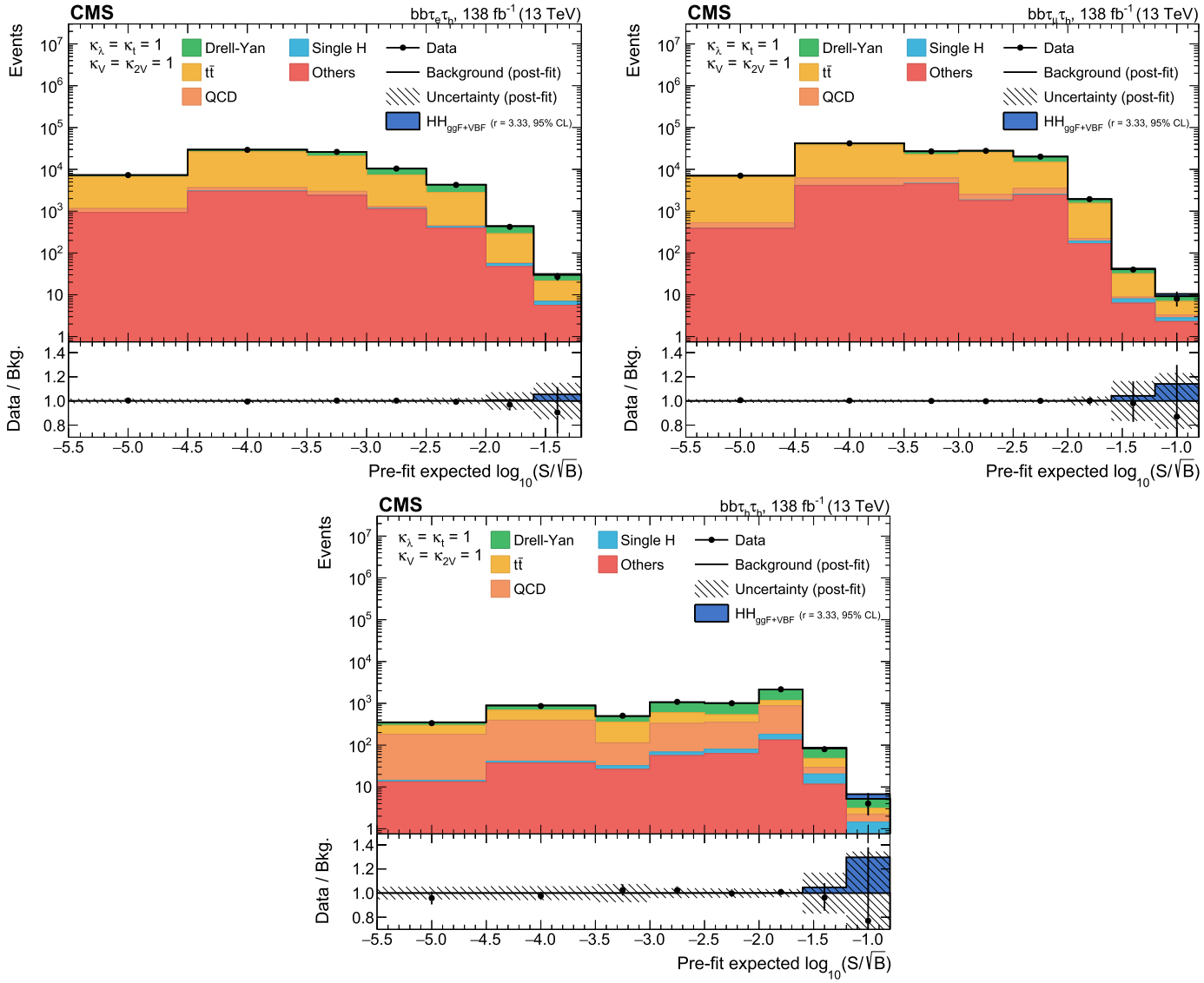

Fig. 5. Combination of bins of all postfit distributions, ordered according to the expected signal-to-square-root-background ratio, where the signal is the SM HH signal expected in that bin and the background is the prefit background estimate in the same bin, separately for the $\tau_e\tau_h$ channel (upper left), the $\tau_\mu\tau_h$ channel (upper right), and $\tau_h\tau_h$ channel (lower). The ratio also shows the signal scaled to the observed exclusion limit (as shown in Table 2).

Table 2
Expected and observed upper limits at 95% CL for the SM point ($\kappa_\lambda = 1$), where $\sigma^{SM}_{ggF+VBF} = 32.776$ fb represents the sum of the ggF plus VBF HH cross sections.

Expected limit	2016	2017	2018	Combined
$\sigma_{ggF+VBF}(pp \to HH)/\sigma^{SM}_{ggF+VBF}$	10.6	11.7	8.2	5.2
$\sigma_{ggF+VBF}(pp \to HH)$ [fb]	324	356	249	159
$\sigma_{ggF+VBF}(pp \to HH \to bb\tau\tau)$ [fb]	23.6	26.0	18.2	11.6
Observed limit	**2016**	**2017**	**2018**	**Combined**
$\sigma_{ggF+VBF}(pp \to HH)/\sigma^{SM}_{ggF+VBF}$	8.9	9.5	5.5	3.3
$\sigma_{ggF+VBF}(pp \to HH)$ [fb]	272	291	169	102
$\sigma_{ggF+VBF}(pp \to HH \to bb\tau\tau)$ [fb]	19.6	21.2	12.4	7.5

Table 3
Expected and observed upper limits at 95% CL for the SM point ($\kappa_{2V} = 1$), where $\sigma^{SM}_{VBF} = 1.726$ fb represents the VBF only HH cross section.

Expected limit	2016	2017	2018	Combined
$\sigma_{VBF}(pp \to qqHH)/\sigma^{SM}_{VBF}$	357	392	226	154
$\sigma_{VBF}(pp \to qqHH)$ [fb]	616	676	391	266
$\sigma_{VBF}(pp \to qqHH \to bb\tau\tau)$ [fb]	45.0	49.3	28.5	19.4
Observed limit	**2016**	**2017**	**2018**	**Combined**
$\sigma_{VBF}(pp \to qqHH)/\sigma^{SM}_{VBF}$	283	280	241	124
$\sigma_{VBF}(pp \to qqHH)$ [fb]	487	485	414	212
$\sigma_{VBF}(pp \to qqHH \to bb\tau\tau)$ [fb]	35.6	35.3	30.2	15.5

listed in Tables 2 and 3, respectively. A visual representation of these limits is provided in Fig. 7.

From limits on the inclusive HH cross section times the $bb\tau\tau$ branching fraction, computed for fixed values of κ_λ following the asymptotic CL_s prescription [65–67], we measure an observed (expected) 95% CL constraint on κ_λ of $-1.7 < \kappa_\lambda < 8.7$ ($-2.9 < \kappa_\lambda < 9.8$). An observed (expected) 95% CL constraint on κ_{2V} of $-0.4 < \kappa_{2V} < 2.6$ ($-0.6 < \kappa_{2V} < 2.8$) is instead deduced from limits on the VBF only HH cross section times the $bb\tau\tau$ branching fraction. The corresponding scans are shown in Fig. 8.

The upper limits are used to set two-dimensional constraints on the coupling modifiers κ_λ, κ_t, κ_{2V}, and κ_V, as shown in Fig. 9. A point in a two-dimensional parameter space is excluded when the upper limit on the overall rate of HH production at 95% CL is measured to be below the theoretical cross section, evaluated at the corresponding parameter values.

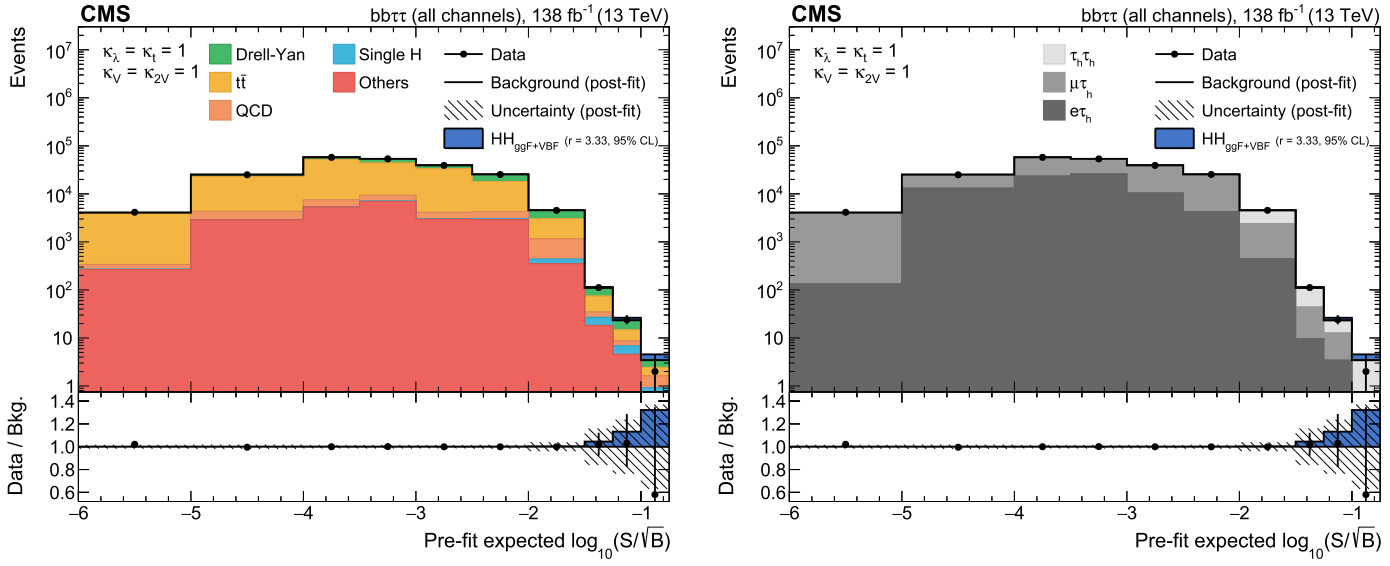

Fig. 6. Combination of bins of all postfit distributions, ordered according to the expected signal-to-square-root-background ratio, where the signal is the SM HH signal expected in that bin and the background is the prefit background estimate in the same bin, separately for the background contribution split into physics processes (left), and split into the three considered final state channels (right). The ratio also shows the signal scaled to the observed exclusion limit (as shown in Table 2).

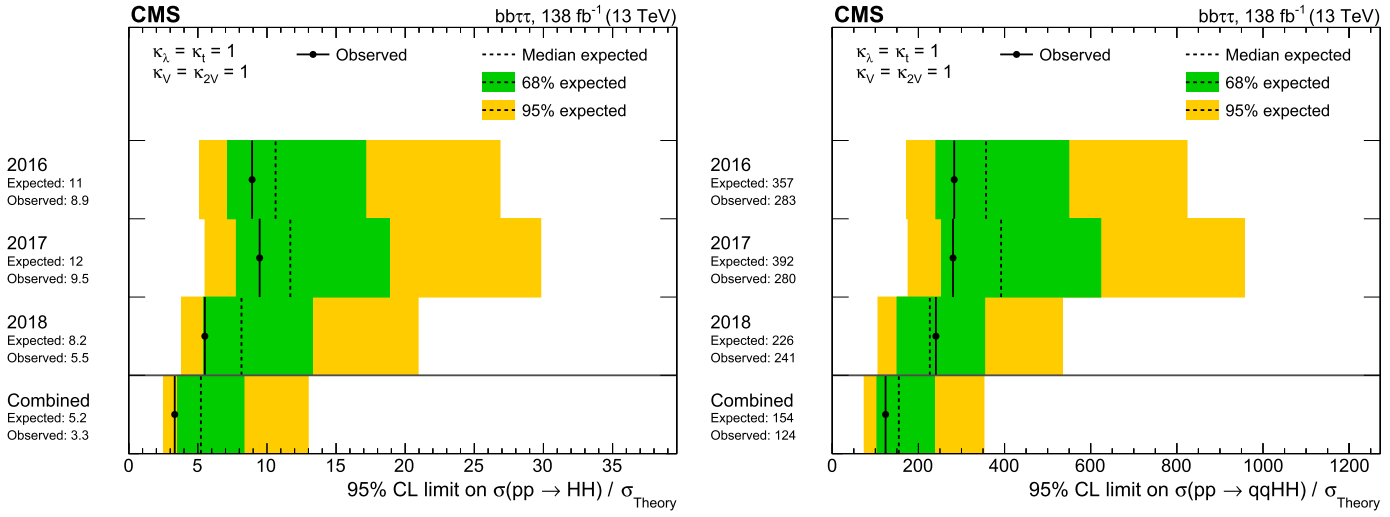

Fig. 7. The expected and observed limits on the ratio of experimentally estimated ggF plus VBF ($\sigma(\mathrm{pp} \to \mathrm{HH})$, left) and VBF only ($\sigma(\mathrm{pp} \to \mathrm{qqHH})$, right) HH production cross section and the expectation from the SM (σ_{Theory}) at 95% CL, separated into different years and combined for the full 2016–2018 data set.

For both the ggF and the VBF results here reported, the largest sensitivity is provided by the $\tau_h\tau_h$ channel, followed by the $\tau_\mu\tau_h$ channel, and lastly by the $\tau_e\tau_h$ one. The resolved categories, especially *res2b*, dominate the sensitivity when measuring the constraint on κ_λ, while the combined VBF multicategories, particularly *classVBF*, provide the most stringent constraints on κ_{2V}.

Assuming that an HH signal exists with the properties predicted by the SM, a scan of the likelihood as a function of the κ_λ and κ_{2V} coupling modifiers is performed, as shown in Fig. 10. This method consists in obtaining central best fit values and confidence intervals for the coupling modifiers directly from the profile likelihood [67], as opposed to using the CL_s method as in the results reported above. The observed confidence interval on κ_λ corresponds to $[+0.68, +6.37]$ at 68% CL and to $[-1.77, +8.73]$ at 95% CL for a best fit value of $\kappa_\lambda = +3.61$. The observed confidence interval on κ_{2V} corresponds to $[+0.28, +1.88]$ at 68% CL and to $[-0.34, +2.49]$ at 95% CL for a best fit value of $\kappa_{2V} = +1.07$.

9. Summary

A search for nonresonant Higgs boson pair (HH) production via gluon-gluon fusion (ggF) and vector boson fusion (VBF) processes in final states with two bottom quarks and two tau leptons was presented. The search uses the full 2016–2018 data set of proton-proton collisions at a center-of-mass energy of $\sqrt{s} = 13\,\mathrm{TeV}$ recorded with the CMS detector at the LHC, corresponding to an integrated luminosity of $138\,\mathrm{fb}^{-1}$. The three decay modes of the $\tau\tau$ pair with the largest branching fraction have been selected, requiring one tau lepton to be always decaying hadronically and the other one either leptonically or hadronically. Upper limits at 95% confidence level (CL) on the inclusive ggF plus VBF HH production cross section are set, as well as on the VBF only HH production cross section.

This analysis benefits from an improved trigger strategy as well as from a series of techniques developed especially for this search: among others, several neural networks to identify the b jets from the H decay, to categorize the events, and to perform signal ex-

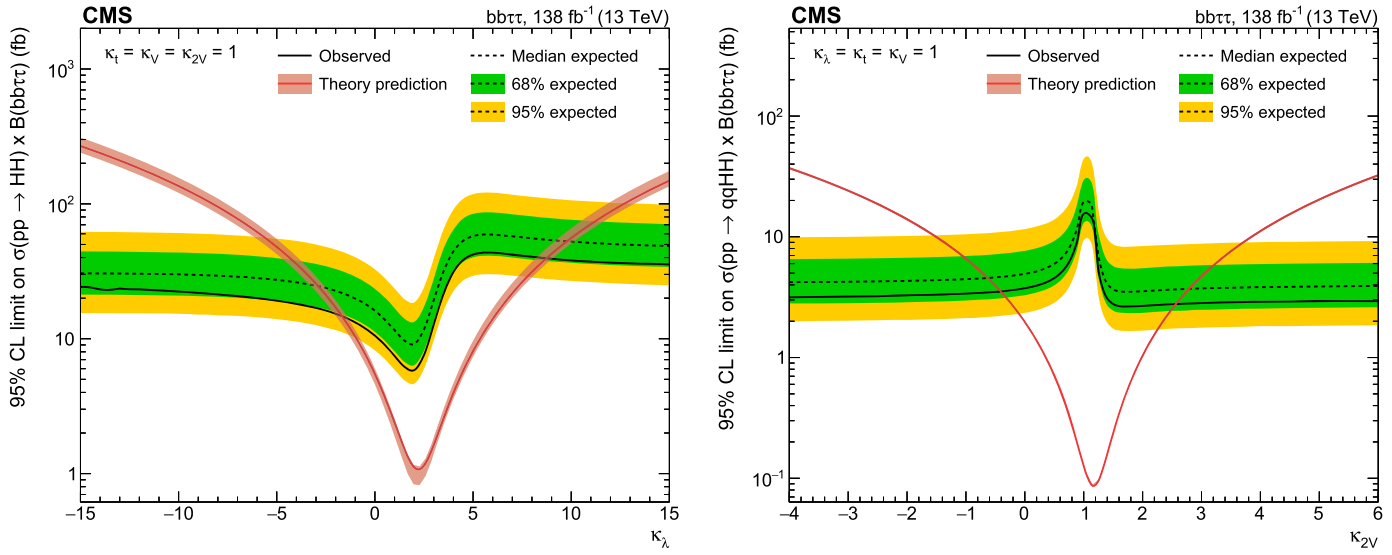

Fig. 8. (left) Observed and expected upper limits at 95% CL as functions of κ_λ on the ggF plus VBF HH cross section times the bb$\tau\tau$ branching fraction. (right) Observed and expected upper limits at 95% CL as functions of κ_{2V} on the VBF only HH cross section times the bb$\tau\tau$ branching fraction. In both cases all other couplings are set to their SM expectation. The red solid line shows the theoretical prediction for the HH production cross section and its uncertainty (red shaded band).

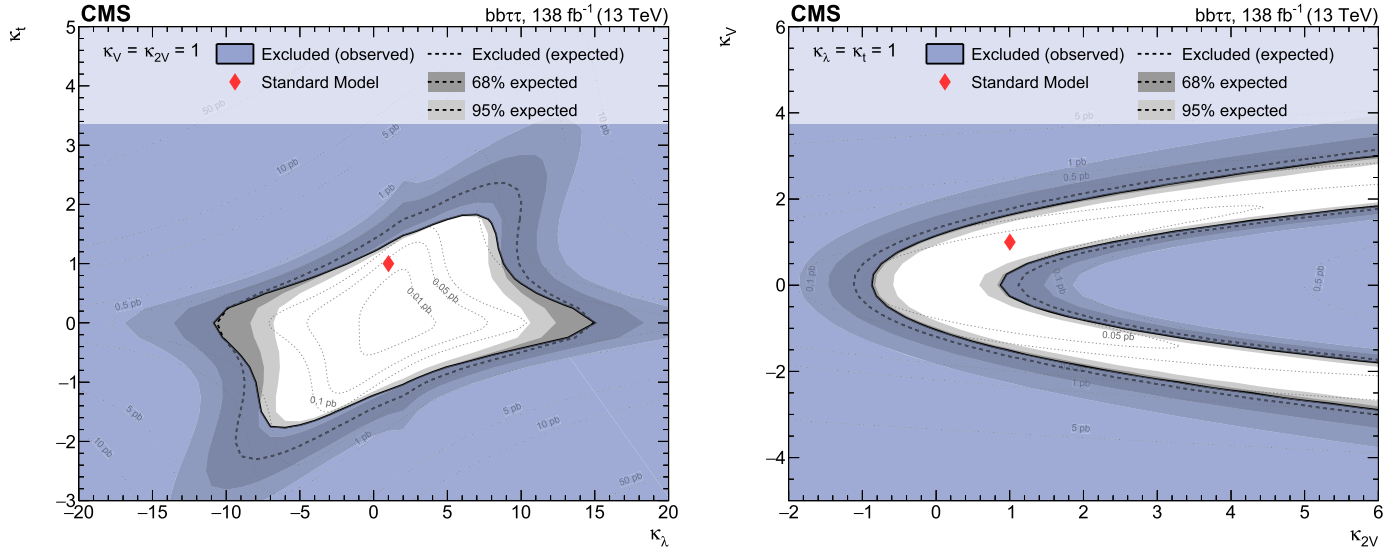

Fig. 9. (left) Two-dimensional exclusion regions as a function of the κ_λ and κ_t couplings for the full 2016–2018 combination, with both κ_{2V} and κ_V are fixed to unity. (right) Two-dimensional exclusion regions as a function of κ_{2V} and κ_V, with both κ_λ and κ_t are set to unity. Expected uncertainties on exclusion boundaries are inferred from uncertainty bands of the limit calculation, and are denoted by dark and light-grey areas. The blue area marks parameter combinations that are observed to be excluded. For visual guidance, theoretical cross section values are illustrated by thin, labeled contour lines with the SM prediction denoted by a red diamond.

traction. Moreover, this analysis builds up on the improvements made by the CMS Collaboration in the jet and tau lepton identification and reconstruction algorithms. All these techniques enable the achievement of particularly stringent results on the HH production cross sections.

The observed (expected) 95% CL upper limit on HH total production cross section corresponds to 3.3 (5.2) times the theoretical SM prediction. The observed (expected) 95% CL upper limit for the VBF only HH SM cross section corresponds to 124 (154) times the theoretical SM prediction.

The observed (expected) 95% CL constraints on κ_λ and κ_{2V}, derived from limits on the HH production cross section times the bb$\tau\tau$ branching fraction, are found to be $-1.7 < \kappa_\lambda < 8.7$ $(-2.9 < \kappa_\lambda < 9.8)$ and $-0.4 < \kappa_{2V} < 2.6$ $(-0.6 < \kappa_{2V} < 2.8)$, respectively.

Declaration of competing interest

The authors declare that they have no known competing financial interests or personal relationships that could have appeared to influence the work reported in this paper.

Data availability

Release and preservation of data used by the CMS Collaboration as the basis for publications is guided by the CMS policy as stated in "CMS data preservation, re-use and open access policy".

Acknowledgements

We congratulate our colleagues in the CERN accelerator departments for the excellent performance of the LHC and thank the

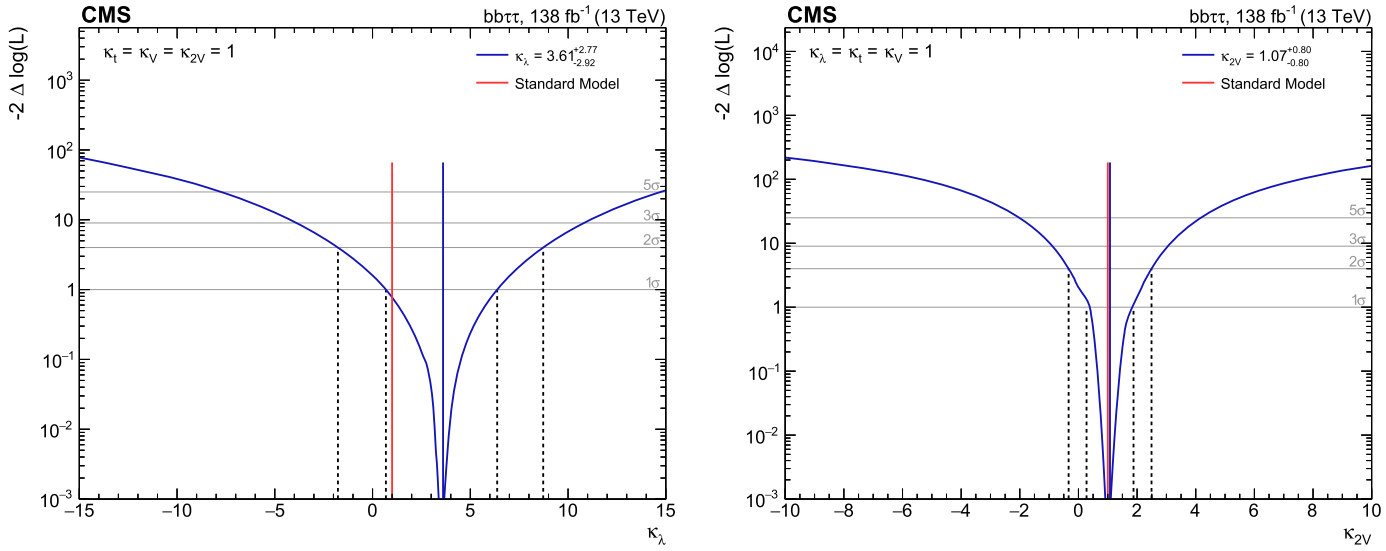

Fig. 10. Observed likelihood scan as a function of κ_λ (left) and κ_{2V} (right) for the full 2016–2018 combination. The dashed lines show the intersection with threshold values one and four, corresponding to 68 and 95% confidence intervals, respectively.

technical and administrative staffs at CERN and at other CMS institutes for their contributions to the success of the CMS effort. In addition, we gratefully acknowledge the computing centers and personnel of the Worldwide LHC Computing Grid and other centers for delivering so effectively the computing infrastructure essential to our analyses. Finally, we acknowledge the enduring support for the construction and operation of the LHC, the CMS detector, and the supporting computing infrastructure provided by the following funding agencies: BMBWF and FWF (Austria); FNRS and FWO (Belgium); CNPq, CAPES, FAPERJ, FAPERGS, and FAPESP (Brazil); MES and BNSF (Bulgaria); CERN; CAS, MOST, and NSFC (China); MINCIENCIAS (Colombia); MSES and CSF (Croatia); RIF (Cyprus); SENESCYT (Ecuador); MoER, ERC PUT and ERDF (Estonia); Academy of Finland, MEC, and HIP (Finland); CEA and CNRS/IN2P3 (France); BMBF, DFG, and HGF (Germany); GSRI (Greece); NKFIH (Hungary); DAE and DST (India); IPM (Iran); SFI (Ireland); INFN (Italy); MSIP and NRF (Republic of Korea); MES (Latvia); LAS (Lithuania); MOE and UM (Malaysia); BUAP, CINVESTAV, CONACYT, LNS, SEP, and UASLP-FAI (Mexico); MOS (Montenegro); MBIE (New Zealand); PAEC (Pakistan); MES and NSC (Poland); FCT (Portugal); MESTD (Serbia); MCIN/AEI and PCTI (Spain); MoSTR (Sri Lanka); Swiss Funding Agencies (Switzerland); MST (Taipei); MHESI and NSTDA (Thailand); TUBITAK and TENMAK (Turkey); NASU (Ukraine); STFC (United Kingdom); DOE and NSF (USA).

Individuals have received support from the Marie-Curie program and the European Research Council and Horizon 2020 Grant, contract Nos. 675440, 724704, 752730, 758316, 765710, 824093, 884104, and COST Action CA16108 (European Union); the Leventis Foundation; the Alfred P. Sloan Foundation; the Alexander von Humboldt Foundation; the Belgian Federal Science Policy Office; the Fonds pour la Formation à la Recherche dans l'Industrie et dans l'Agriculture (FRIA-Belgium); the Agentschap voor Innovatie door Wetenschap en Technologie (IWT-Belgium); the F.R.S.-FNRS and FWO (Belgium) under the "Excellence of Science – EOS" – be.h project n. 30820817; the Beijing Municipal Science & Technology Commission, No. Z191100007219010; The Ministry of Education, Youth and Sports (MEYS) of the Czech Republic; the Hellenic Foundation for Research and Innovation (HFRI), Project Number 2288 (Greece); the Deutsche Forschungsgemeinschaft (DFG), under Germany's Excellence Strategy – EXC 2121 "Quantum Universe" – 390833306, and under project number 400140256 - GRK2497; the Hungarian Academy of Sciences, the New National Excellence Program - ÚNKP, the NKFIH research grants K 124845, K 124850, K 128713, K 128786, K 129058, K 131991, K 133046, K 138136, K 143460, K 143477, 2020-2.2.1-ED-2021-00181, and TKP2021-NKTA-64 (Hungary); the Council of Science and Industrial Research, India; the Latvian Council of Science; the Ministry of Education and Science, project no. 2022/WK/14, and the National Science Center, contracts Opus 2021/41/B/ST2/01369 and 2021/43/B/ST2/01552 (Poland); the Fundação para a Ciência e a Tecnologia, grant CEECIND/01334/2018 (Portugal); the National Priorities Research Program by Qatar National Research Fund; MCIN/AEI/10.13039/501100011033, ERDF "a way of making Europe", and the Programa Estatal de Fomento de la Investigación Científica y Técnica de Excelencia María de Maeztu, grant MDM-2017-0765 and Programa Severo Ochoa del Principado de Asturias (Spain); the Chulalongkorn Academic into Its 2nd Century Project Advancement Project, and the National Science, Research and Innovation Fund via the Program Management Unit for Human Resources & Institutional Development, Research and Innovation, grant B05F650021 (Thailand); the Kavli Foundation; the Nvidia Corporation; the SuperMicro Corporation; the Welch Foundation, contract C-1845; and the Weston Havens Foundation (USA).

References

[1] ATLAS Collaboration, Observation of a new particle in the search for the Standard Model Higgs boson with the ATLAS detector at the LHC, Phys. Lett. B 716 (2012) 1, https://doi.org/10.1016/j.physletb.2012.08.020, arXiv:1207.7214.

[2] CMS Collaboration, Observation of a new boson at a mass of 125 GeV with the CMS experiment at the LHC, Phys. Lett. B 716 (2012) 30, https://doi.org/10.1016/j.physletb.2012.08.021, arXiv:1207.7235.

[3] CMS Collaboration, Observation of a new boson with mass near 125 GeV in proton-proton collisions at $\sqrt{s} = 7$ and 8 TeV, J. High Energy Phys. 06 (2013) 081, https://doi.org/10.1007/JHEP06(2013)081, arXiv:1303.4571.

[4] CMS Collaboration, A measurement of the Higgs boson mass in the diphoton decay channel, Phys. Lett. B 805 (2020) 135425, https://doi.org/10.1016/j.physletb.2020.135425, arXiv:2002.06398.

[5] G. Aad, et al., C.M.S. ATLAS, Measurements of the Higgs boson production and decay rates and constraints on its couplings from a combined ATLAS and CMS analysis of the LHC proton-proton collision data at $\sqrt{s} = 7$ and 8 TeV, J. High Energy Phys. 08 (2016) 045, https://doi.org/10.1007/JHEP08(2016)045, arXiv:1606.02266.

[6] M. Grazzini, G. Heinrich, S. Jones, S. Kallweit, M. Kerner, J.M. Lindert, J. Mazzitelli, Higgs boson pair production at NNLO with top quark mass effects, J. High Energy Phys. 05 (2018) 59, https://doi.org/10.1007/jhep05(2018)059, arXiv:1803.02463.

[7] J. Baglio, F. Campanario, S. Glaus, M. Múhlleitner, J. Ronca, M. Spira, $gg \to HH$: combined uncertainties, Phys. Rev. D 103 (2021) 056002, https://doi.org/10.1103/PhysRevD.103.056002, arXiv:2008.11626v3.

[8] F.A. Dreyer, A. Karlberg, Vector-boson fusion Higgs pair production at N^{3}LO, Phys. Rev. D 98 (2018) 114016, https://doi.org/10.1103/PhysRevD.98.114016, arXiv:1811.07906.

[9] B. Di Micco, M. Gouzevitch, J. Mazzitelli, C. Vernieri, J. Alison, K. Androsov, J. Baglio, E. Bagnaschi, S. Banerjee, P. Basler, A. Bethani, A. Betti, M. Blanke, A. Blondel, L. Borgonovi, et al., Higgs boson pair production at colliders: status and perspectives, Rev. Phys. 5 (2020) 100045, https://doi.org/10.1016/j.revip.2020.100045, arXiv:1910.00012.

[10] CMS Collaboration, Identification of hadronic tau lepton decays using a deep neural network, J. Instrum. 17 (2022) P07023, https://doi.org/10.1088/1748-0221/17/07/P07023, arXiv:2201.08458, submitted for publication.

[11] CMS Collaboration, Search for Higgs boson pair production in events with two bottom quarks and two tau leptons in proton-proton collisions at $\sqrt{s} = 13$ TeV, Phys. Lett. B 778 (2017) 101, https://doi.org/10.1016/j.physletb.2018.01.001, arXiv:1707.02909.

[12] ATLAS Collaboration, Search for resonant and nonresonant Higgs boson pair production in the $b\bar{b}\tau^+\tau^-$ decay channel in proton-proton collisions at $\sqrt{s} = 13$ TeV with the ATLAS detector, Phys. Rev. Lett. 121 (2018) 191801, https://doi.org/10.1103/PhysRevLett.121.191801, arXiv:1808.00336.

[13] E. Bols, J. Kieseler, M. Verzetti, M. Stoye, A. Stakia, Jet flavour classification using DeepJet, J. Instrum. 15 (2020) P12012, https://doi.org/10.1088/1748-0221/15/12/p12012, arXiv:2008.10519.

[14] HEPData record for this analysis, https://doi.org/10.17182/hepdata.127767, 2022.

[15] CMS Collaboration, Performance of the CMS level-1 trigger in proton-proton collisions at $\sqrt{s} = 13$ TeV, J. Instrum. 15 (2020) P10017, https://doi.org/10.1088/1748-0221/15/10/P10017, arXiv:2006.10165.

[16] CMS Collaboration, The CMS trigger system, J. Instrum. 12 (2017) P01020, https://doi.org/10.1088/1748-0221/12/01/P01020, arXiv:1609.02366.

[17] CMS Collaboration, The CMS experiment at the CERN LHC, J. Instrum. 3 (2008) S08004, https://doi.org/10.1088/1748-0221/3/08/S08004.

[18] CMS Collaboration, Precision luminosity measurement in proton-proton collisions at $\sqrt{s} = 13$ TeV in 2015 and 2016 at CMS, Eur. Phys. J. C 81 (2021) 800, https://doi.org/10.1140/epjc/s10052-021-09538-2, arXiv:2104.01927.

[19] CMS Collaboration, CMS Luminosity Measurement for the 2017 Data-Taking Period at $\sqrt{s} = 13$ TeV, CMS Physics Analysis Summary CMS-PAS-LUM-17-004, CERN, 2017, https://cds.cern.ch/record/2621960.

[20] CMS Collaboration, CMS luminosity measurement for the 2018 data-taking period at $\sqrt{s} = 13$ TeV, CMS Physics Analysis Summary CMS-PAS-LUM-18-002, CERN, 2019, https://cds.cern.ch/record/2676164.

[21] J. Alwall, R. Frederix, S. Frixione, V. Hirschi, F. Maltoni, O. Mattelaer, H.-S. Shao, T. Stelzer, P. Torrielli, M. Zaro, The automated computation of tree-level and next-to-leading order differential cross sections, and their matching to parton shower simulations, J. High Energy Phys. 07 (2014) 79, https://doi.org/10.1007/jhep07(2014)079, arXiv:1405.0301.

[22] S. Frixione, P. Nason, C. Oleari, Matching NLO QCD computations with parton shower simulations: the POWHEG method, J. High Energy Phys. 11 (2007) 070, https://doi.org/10.1088/1126-6708/2007/11/070, arXiv:0709.2092.

[23] E. Re, Single-top Wt-channel production matched with parton showers using the POWHEG method, Eur. Phys. J. C 71 (2011) 1547, https://doi.org/10.1140/epjc/s10052-011-1547-z, arXiv:1009.2450.

[24] J.M. Campbell, R.K. Ellis, P. Nason, E. Re, Top-pair production and decay at NLO matched with parton showers, J. High Energy Phys. 04 (2015) 114, https://doi.org/10.1007/jhep04(2015)114, arXiv:1412.1828.

[25] G. Heinrich, S.P. Jones, M. Kerner, G. Luisoni, L. Scyboz, Probing the trilinear Higgs boson coupling in di-Higgs production at NLO QCD including parton shower effects, J. High Energy Phys. 06 (2019) 66, https://doi.org/10.1007/JHEP06(2019)066, arXiv:1903.08137.

[26] J. Alwall, S. Höche, F. Krauss, N. Lavesson, L. Lönnblad, F. Maltoni, M.L. Mangano, M. Moretti, C.G. Papadopoulos, F. Piccinini, S. Schumann, M. Treccani, J. Winter, M. Worek, Comparative study of various algorithms for the merging of parton showers and matrix elements in hadronic collisions, Eur. Phys. J. C 53 (2007) 473, https://doi.org/10.1140/epjc/s10052-007-0490-5, arXiv:0706.2569.

[27] R. Frederix, S. Frixione, Merging meets matching in MC@NLO, J. High Energy Phys. 12 (2012) 61, https://doi.org/10.1007/jhep12(2012)061, arXiv:1209.6215.

[28] T. Sjöstrand, S. Ask, J.R. Christiansen, R. Corke, N. Desai, P. Ilten, S. Mrenna, S. Prestel, C.O. Rasmussen, P.Z. Skands, An introduction to PYTHIA 8.2, Comput. Phys. Commun. 191 (2015) 159, https://doi.org/10.1016/j.cpc.2015.01.024, arXiv:1410.3012.

[29] CMS Collaboration, Event generator tunes obtained from underlying event and multiparton scattering measurements, Eur. Phys. J. C 76 (2016) 155, https://doi.org/10.1140/epjc/s10052-016-3988-x, arXiv:1512.00815.

[30] CMS Collaboration, Extraction and validation of a new set of CMS PYTHIA8 tunes from underlying-event measurements, Eur. Phys. J. C 80 (2020) 4, https://doi.org/10.1140/epjc/s10052-019-7499-4, arXiv:1903.12179.

[31] R.D. Ball, V. Bertone, S. Carrazza, C.S. Deans, L. Del Debbio, S. Forte, A. Guffanti, N.P. Hartland, J. Latorre, J. Rojo, M. Ubiali, T.N. collaboration, Parton distributions for the LHC run II, J. High Energy Phys. 04 (2015) 40, https://doi.org/10.1007/JHEP04(2015)040, arXiv:1410.8849.

[32] R.D. Ball, V. Bertone, S. Carrazza, L.D. Debbio, S. Forte, P. Groth-Merrild, A. Guffanti, N.P. Hartland, Z. Kassabov, J. Latorre, E.R. Nocera, J. Rojo, L. Rottoli, E. Slade, M. Ubiali, Parton distributions from high-precision collider data, Eur. Phys. J. C 77 (2017) 663, https://doi.org/10.1140/epjc/s10052-017-5199-5, arXiv:1706.00428.

[33] S. Agostinelli, et al., GEANT4, GEANT4—a simulation toolkit, Nucl. Instrum. Methods A 506 (2003) 250, https://doi.org/10.1016/S0168-9002(03)01368-8.

[34] CMS Collaboration, Particle-flow reconstruction and global event description with the CMS detector, J. Instrum. 12 (2017) P10003, https://doi.org/10.1088/1748-0221/12/10/P10003, arXiv:1706.04965.

[35] CMS Collaboration, Performance of missing transverse momentum reconstruction in proton-proton collisions at $\sqrt{s} = 13$ TeV using the CMS detector, J. Instrum. 14 (2019) P07004, https://doi.org/10.1088/1748-0221/14/07/P07004, arXiv:1903.06078.

[36] CMS Collaboration, Technical Proposal for the Phase-II Upgrade of the Compact Muon Solenoid, CMS Technical Proposal CERN-LHCC-2015-010, CMS-TDR-15-02, CERN, 2015, http://cds.cern.ch/record/2020886.

[37] CMS Collaboration, Electron and photon reconstruction and identification with the CMS experiment at the CERN LHC, J. Instrum. 16 (2021) P05014, https://doi.org/10.1088/1748-0221/16/05/P05014, arXiv:2012.06888.

[38] CMS Collaboration, ECAL 2016 Refined Calibration and Run2 Summary Plots, CMS Detector Performance Summary CMS-DP-2020-021, CERN, 2020, https://cds.cern.ch/record/2717925.

[39] CMS Collaboration, Performance of the CMS muon detector and muon reconstruction with proton-proton collisions at $\sqrt{s} = 13$ TeV, J. Instrum. 13 (2018) P06015, https://doi.org/10.1088/1748-0221/13/06/P06015, arXiv:1804.04528.

[40] CMS Collaboration, Performance of τ-lepton reconstruction and identification in CMS, J. Instrum. 7 (2012) P01001, https://doi.org/10.1088/1748-0221/7/01/P01001, arXiv:1109.6034.

[41] CMS Collaboration, Reconstruction and identification of τ lepton decays to hadrons and ν_τ at CMS, J. Instrum. 11 (2016) P01019, https://doi.org/10.1088/1748-0221/11/01/P01019, arXiv:1510.07488.

[42] CMS Collaboration, Performance of reconstruction and identification of τ leptons decaying to hadrons and ν_τ in proton-proton collisions at $\sqrt{s} = 13$ TeV, J. Instrum. 13 (2018) P10005, https://doi.org/10.1088/1748-0221/13/10/P10005, arXiv:1809.02816.

[43] M. Cacciari, G.P. Salam, G. Soyez, The anti-k_T jet clustering algorithm, J. High Energy Phys. 04 (2008) 063, https://doi.org/10.1088/1126-6708/2008/04/063, arXiv:0802.1189.

[44] M. Cacciari, G.P. Salam, G. Soyez, FastJet user manual, Eur. Phys. J. C 72 (2012) 1896, https://doi.org/10.1140/epjc/s10052-012-1896-2, arXiv:1111.6097.

[45] Y.L. Dokshitzer, G.D. Leder, S. Moretti, B.R. Webber, Better jet clustering algorithms, J. High Energy Phys. 08 (1997) 001, https://doi.org/10.1088/1126-6708/1997/08/001, arXiv:hep-ph/9707323.

[46] M. Wobisch, T. Wengler, Hadronization corrections to jet cross-sections in deep inelastic scattering, in: Proceedings of the Workshop on Monte Carlo Generators for HERA Physics, Hamburg, Germany, 1998, p. 270, https://inspirehep.net/record/484872, arXiv:hep-ph/9907280.

[47] M. Dasgupta, A. Fregoso, S. Marzani, G.P. Salam, Towards an understanding of jet substructure, J. High Energy Phys. 09 (2013) 029, https://doi.org/10.1007/JHEP09(2013)029, arXiv:1307.0007.

[48] J.M. Butterworth, A.R. Davison, M. Rubin, G.P. Salam, Jet substructure as a new Higgs search channel at the LHC, Phys. Rev. Lett. 100 (2008) 242001, https://doi.org/10.1103/PhysRevLett.100.242001, arXiv:0802.2470.

[49] CMS Collaboration, Pileup mitigation at CMS in $\sqrt{s} = 13$ TeV data, J. Instrum. 15 (2020) P09018, https://doi.org/10.1088/1748-0221/15/09/p09018, arXiv:2003.00503.

[50] D. Bertolini, P. Harris, M. Low, N. Tran, Pileup per particle identification, J. High Energy Phys. 10 (2014) 059, https://doi.org/10.1007/JHEP10(2014)059, arXiv:1407.6013.

[51] CMS Collaboration, Jet energy scale and resolution in the CMS experiment in proton-proton collisions at $\sqrt{s} = 8$ TeV, J. Instrum. 12 (2017) P02014, https://doi.org/10.1088/1748-0221/12/02/P02014, arXiv:1607.03663.

[52] CMS Collaboration, Jet Energy Scale and Resolution Measurement with Run-2 Legacy Data Collected by CMS at $\sqrt{s} = 13$ TeV, CMS Detector Performance Summary CMS-DP-2021-033, CERN, 2021, https://cds.cern.ch/record/2792322.

[53] L. Bianchini, J. Conway, E.K. Friis, C. Veelken, Reconstruction of the Higgs mass in $H \to \tau\tau$ events by dynamical likelihood techniques, J. Phys. Conf. Ser. 513 (2014) 022035, https://doi.org/10.1088/1742-6596/513/2/022035.

[54] G.C. Strong, On the impact of selected modern deep-learning techniques to the performance and celerity of classification models in an experimental high-energy physics use case, Mach. Learn.: Sci. Technol. (2020), https://doi.org/10.1088/2632-2153/ab983a, arXiv:2002.01427.

[55] S.J. Hanson, A stochastic version of the delta rule, Physica D 42 (1990) 265, https://doi.org/10.1016/0167-2789(90)90081-Y.

[56] N. Srivastava, G. Hinton, A. Krizhevsky, I. Sutskever, R. Salakhutdinov, Dropout: a simple way to prevent neural networks from overfitting, J. Mach. Learn. Res. 15 (2014) 1929, http://jmlr.org/papers/v15/srivastava14a.html.

[57] F. Rosenblatt, The perceptron: a probabilistic model for information storage and organization in the brain, Psychol. Rev. 65 (1957) 386, https://doi.org/10.1037/h0042519.

[58] S. Linnainmaa, Taylor expansion of the accumulated rounding error, BIT Numer. Math. 16 (1976) 146, https://doi.org/10.1007/BF01931367.
[59] P.J. Werbos, Applications of advances in nonlinear sensitivity analysis, in: Proc. 10th IFIP Conf., 31/8–4/9, NYC, 1981, p. 762.
[60] D.E. Rumelhart, G.E. Hinton, R.J. Williams, Learning representations by back-propagating errors, Nature 323 (1986) 533, https://doi.org/10.1038/323533a0.
[61] CMS Collaboration, Prospects for HH Measurements at the HL-LHC, CMS Physics Analysis Summary CMS-PAS-FTR-18-019, CERN, Geneva, 2018, https://cds.cern.ch/record/2652549.
[62] E.M. Cepeda, S. Gori, P. Ilten, M. Kado, F. Riva, Higgs physics at the HL-LHC and HE-LHC, CERN Yellow Rep. Monogr. 7 (2018) 221, https://doi.org/10.23731/CYRM-2019-007.221, arXiv:1902.00134.
[63] D. de Florian, et al., Handbook of LHC Higgs cross sections: 4. Deciphering the nature of the Higgs sector, CERN Yellow Rep. Monogr. 2 (2017) 21, https://doi.org/10.23731/CYRM-2017-002, arXiv:1610.07922.
[64] B. Cabouat, T. Sjöstrand, Some dipole shower studies, Eur. Phys. J. C 78 (2018) 226, https://doi.org/10.1140/epjc/s10052-018-5645-z, arXiv:1710.00391v2.
[65] T. Junk, Confidence level computation for combining searches with small statistics, Nucl. Instrum. Methods A 434 (1999) 435, https://doi.org/10.1016/S0168-9002(99)00498-2, arXiv:hep-ex/9902006.
[66] A.L. Read, Presentation of search results: the CL_s technique, J. Phys. G 28 (2002) 2693, https://doi.org/10.1088/0954-3899/28/10/313.
[67] G. Cowan, K. Cranmer, E. Gross, O. Vitells, Asymptotic formulae for likelihood-based tests of new physics, Eur. Phys. J. C 71 (2011) 1554, https://doi.org/10.1140/epjc/s10052-011-1554-0, arXiv:1007.1727, [Erratum: https://doi.org/10.1140/epjc/s10052-013-2501-z].
[68] J.B. Močkus, L.J. Močkus, Bayesian approach to global optimization and application to multiobjective and constrained problems, J. Optim. Theory Appl. 70 (1991) 157, https://doi.org/10.1007/BF00940509, arXiv:2108.00002.

The CMS collaboration

A. Tumasyan [1]

Yerevan Physics Institute, Yerevan, Armenia

W. Adam, J.W. Andrejkovic, T. Bergauer, S. Chatterjee, K. Damanakis, M. Dragicevic, A. Escalante Del Valle, P.S. Hussain, M. Jeitler [2], N. Krammer, L. Lechner, D. Liko, I. Mikulec, P. Paulitsch, F.M. Pitters, J. Schieck [2], R. Schöfbeck, D. Schwarz, S. Templ, W. Waltenberger, C.-E. Wulz [2]

Institut für Hochenergiephysik, Vienna, Austria

M.R. Darwish [3], T. Janssen, T. Kello [4], H. Rejeb Sfar, P. Van Mechelen

Universiteit Antwerpen, Antwerpen, Belgium

E.S. Bols, J. D'Hondt, A. De Moor, M. Delcourt, H. El Faham, S. Lowette, S. Moortgat, A. Morton, D. Müller, A.R. Sahasransu, S. Tavernier, W. Van Doninck, D. Vannerom

Vrije Universiteit Brussel, Brussel, Belgium

B. Clerbaux, G. De Lentdecker, L. Favart, J. Jaramillo, K. Lee, M. Mahdavikhorrami, I. Makarenko, A. Malara, S. Paredes, L. Pétré, N. Postiau, E. Starling, L. Thomas, M. Vanden Bemden, C. Vander Velde, P. Vanlaer

Université Libre de Bruxelles, Bruxelles, Belgium

D. Dobur, J. Knolle, L. Lambrecht, G. Mestdach, M. Niedziela, C. Rendón, C. Roskas, A. Samalan, K. Skovpen, M. Tytgat, N. Van Den Bossche, B. Vermassen, L. Wezenbeek

Ghent University, Ghent, Belgium

A. Benecke, A. Bethani, G. Bruno, F. Bury, C. Caputo, P. David, C. Delaere, I.S. Donertas, A. Giammanco, K. Jaffel, Sa. Jain, V. Lemaitre, K. Mondal, J. Prisciandaro, A. Taliercio, T.T. Tran, P. Vischia, S. Wertz

Université Catholique de Louvain, Louvain-la-Neuve, Belgium

G.A. Alves, E. Coelho, C. Hensel, A. Moraes, P. Rebello Teles

Centro Brasileiro de Pesquisas Fisicas, Rio de Janeiro, Brazil

W.L. Aldá Júnior, M. Alves Gallo Pereira, M. Barroso Ferreira Filho, H. Brandao Malbouisson, W. Carvalho, J. Chinellato [5], E.M. Da Costa, G.G. Da Silveira [6], D. De Jesus Damiao, V. Dos Santos Sousa, S. Fonseca De Souza, J. Martins [7], C. Mora Herrera, K. Mota Amarilo, L. Mundim, H. Nogima, A. Santoro, S.M. Silva Do Amaral, A. Sznajder, M. Thiel, F. Torres Da Silva De Araujo [8], A. Vilela Pereira

Universidade do Estado do Rio de Janeiro, Rio de Janeiro, Brazil

C.A. Bernardes [6], L. Calligaris, T.R. Fernandez Perez Tomei, E.M. Gregores, P.G. Mercadante, S.F. Novaes, Sandra S. Padula

Universidade Estadual Paulista, Universidade Federal do ABC, São Paulo, Brazil

A. Aleksandrov, G. Antchev, R. Hadjiiska, P. Iaydjiev, M. Misheva, M. Rodozov, M. Shopova, G. Sultanov

Institute for Nuclear Research and Nuclear Energy, Bulgarian Academy of Sciences, Sofia, Bulgaria

A. Dimitrov, T. Ivanov, L. Litov, B. Pavlov, P. Petkov, A. Petrov, E. Shumka

University of Sofia, Sofia, Bulgaria

T. Cheng, T. Javaid [9], M. Mittal, L. Yuan

Beihang University, Beijing, China

M. Ahmad, G. Bauer [10], Z. Hu, S. Lezki, K. Yi [10,11]

Department of Physics, Tsinghua University, Beijing, China

G.M. Chen [9], H.S. Chen [9], M. Chen [9], F. Iemmi, C.H. Jiang, A. Kapoor, H. Liao, Z.-A. Liu [12], V. Milosevic, F. Monti, R. Sharma, J. Tao, J. Thomas-Wilsker, J. Wang, H. Zhang, J. Zhao

Institute of High Energy Physics, Beijing, China

A. Agapitos, Y. An, Y. Ban, C. Chen, A. Levin, C. Li, Q. Li, X. Lyu, Y. Mao, S.J. Qian, X. Sun, D. Wang, J. Xiao, H. Yang

State Key Laboratory of Nuclear Physics and Technology, Peking University, Beijing, China

J. Li, M. Lu, Z. You

Sun Yat-Sen University, Guangzhou, China

X. Gao [4], D. Leggat, H. Okawa, Y. Zhang

Institute of Modern Physics and Key Laboratory of Nuclear Physics and Ion-beam Application (MOE) – Fudan University, Shanghai, China

Z. Lin, C. Lu, M. Xiao

Zhejiang University, Hangzhou, Zhejiang, China

C. Avila, D.A. Barbosa Trujillo, A. Cabrera, C. Florez, J. Fraga

Universidad de Los Andes, Bogota, Colombia

J. Mejia Guisao, F. Ramirez, M. Rodriguez, J.D. Ruiz Alvarez

Universidad de Antioquia, Medellin, Colombia

D. Giljanovic, N. Godinovic, D. Lelas, I. Puljak

University of Split, Faculty of Electrical Engineering, Mechanical Engineering and Naval Architecture, Split, Croatia

Z. Antunovic, M. Kovac, T. Sculac

University of Split, Faculty of Science, Split, Croatia

V. Brigljevic, B.K. Chitroda, D. Ferencek, D. Majumder, M. Roguljic, A. Starodumov [13], T. Susa

Institute Rudjer Boskovic, Zagreb, Croatia

A. Attikis, K. Christoforou, G. Kole, M. Kolosova, S. Konstantinou, J. Mousa, C. Nicolaou, F. Ptochos, P.A. Razis, H. Rykaczewski, H. Saka

University of Cyprus, Nicosia, Cyprus

M. Finger [13], M. Finger Jr. [13], A. Kveton

Charles University, Prague, Czech Republic

E. Ayala

Escuela Politecnica Nacional, Quito, Ecuador

E. Carrera Jarrin

Universidad San Francisco de Quito, Quito, Ecuador

Y. Assran [14,15], S. Elgammal [15]

Academy of Scientific Research and Technology of the Arab Republic of Egypt, Egyptian Network of High Energy Physics, Cairo, Egypt

A. Lotfy, M.A. Mahmoud

Center for High Energy Physics (CHEP-FU), Fayoum University, El-Fayoum, Egypt

S. Bhowmik, R.K. Dewanjee, K. Ehataht, M. Kadastik, S. Nandan, C. Nielsen, J. Pata, M. Raidal, L. Tani, C. Veelken

National Institute of Chemical Physics and Biophysics, Tallinn, Estonia

P. Eerola, H. Kirschenmann, K. Osterberg, M. Voutilainen

Department of Physics, University of Helsinki, Helsinki, Finland

S. Bharthuar, E. Brücken, F. Garcia, J. Havukainen, M.S. Kim, R. Kinnunen, T. Lampén, K. Lassila-Perini, S. Lehti, T. Lindén, M. Lotti, L. Martikainen, M. Myllymäki, J. Ott, M.m. Rantanen, H. Siikonen, E. Tuominen, J. Tuominiemi

Helsinki Institute of Physics, Helsinki, Finland

P. Luukka, H. Petrow, T. Tuuva

Lappeenranta-Lahti University of Technology, Lappeenranta, Finland

C. Amendola, M. Besancon, F. Couderc, M. Dejardin, D. Denegri, J.L. Faure, F. Ferri, S. Ganjour, P. Gras, G. Hamel de Monchenault, P. Jarry, V. Lohezic, J. Malcles, J. Rander, A. Rosowsky, M.Ö. Sahin, A. Savoy-Navarro [16], P. Simkina, M. Titov

IRFU, CEA, Université Paris-Saclay, Gif-sur-Yvette, France

C. Baldenegro Barrera, F. Beaudette, A. Buchot Perraguin, P. Busson, A. Cappati, C. Charlot, O. Davignon, B. Diab, G. Falmagne, B.A. Fontana Santos Alves, S. Ghosh, R. Granier de Cassagnac, A. Hakimi, B. Harikrishnan, J. Motta, M. Nguyen, C. Ochando, L. Portales, J. Rembser, R. Salerno, U. Sarkar, J.B. Sauvan, Y. Sirois, A. Tarabini, E. Vernazza, A. Zabi, A. Zghiche

Laboratoire Leprince-Ringuet, CNRS/IN2P3, Ecole Polytechnique, Institut Polytechnique de Paris, Palaiseau, France

J.-L. Agram [17], J. Andrea, D. Apparu, D. Bloch, G. Bourgatte, J.-M. Brom, E.C. Chabert, C. Collard, D. Darej, U. Goerlach, C. Grimault, A.-C. Le Bihan, P. Van Hove

Université de Strasbourg, CNRS, IPHC UMR 7178, Strasbourg, France

S. Beauceron, C. Bernet, G. Boudoul, C. Camen, A. Carle, N. Chanon, J. Choi, D. Contardo, P. Depasse, C. Dozen [18], H. El Mamouni, J. Fay, S. Gascon, M. Gouzevitch, G. Grenier, B. Ille, I.B. Laktineh, M. Lethuillier, L. Mirabito, S. Perries, K. Shchablo, V. Sordini, L. Torterotot, M. Vander Donckt, P. Verdier, S. Viret

Institut de Physique des 2 Infinis de Lyon (IP2I), Villeurbanne, France

D. Chokheli, I. Lomidze, Z. Tsamalaidze [13]

Georgian Technical University, Tbilisi, Georgia

V. Botta, L. Feld, K. Klein, M. Lipinski, D. Meuser, A. Pauls, N. Röwert, M. Teroerde

RWTH Aachen University, I. Physikalisches Institut, Aachen, Germany

S. Diekmann, A. Dodonova, N. Eich, D. Eliseev, M. Erdmann, P. Fackeldey, B. Fischer, T. Hebbeker, K. Hoepfner, F. Ivone, M.y. Lee, L. Mastrolorenzo, M. Merschmeyer, A. Meyer, S. Mondal, S. Mukherjee, D. Noll, A. Novak, F. Nowotny, A. Pozdnyakov, Y. Rath, W. Redjeb, H. Reithler, A. Schmidt, S.C. Schuler, A. Sharma, L. Vigilante, S. Wiedenbeck, S. Zaleski

RWTH Aachen University, III. Physikalisches Institut A, Aachen, Germany

C. Dziwok, G. Flügge, W. Haj Ahmad [19], O. Hlushchenko, T. Kress, A. Nowack, O. Pooth, A. Stahl [20], T. Ziemons, A. Zotz

RWTH Aachen University, III. Physikalisches Institut B, Aachen, Germany

H. Aarup Petersen, M. Aldaya Martin, P. Asmuss, S. Baxter, M. Bayatmakou, O. Behnke, A. Bermúdez Martínez, S. Bhattacharya, A.A. Bin Anuar, F. Blekman [21], K. Borras [22], D. Brunner, A. Campbell, A. Cardini, C. Cheng, F. Colombina, S. Consuegra Rodríguez, G. Correia Silva, M. De Silva, L. Didukh, G. Eckerlin, D. Eckstein, L.I. Estevez Banos, O. Filatov, E. Gallo [21], A. Geiser, A. Giraldi, G. Greau, A. Grohsjean, V. Guglielmi, M. Guthoff, A. Jafari [23], N.Z. Jomhari, B. Kaech, A. Kasem [22], M. Kasemann, H. Kaveh, C. Kleinwort, R. Kogler, M. Komm, D. Krücker, W. Lange, D. Leyva Pernia, K. Lipka, W. Lohmann [24], R. Mankel, I.-A. Melzer-Pellmann, M. Mendizabal Morentin, J. Metwally, A.B. Meyer, G. Milella, M. Mormile, A. Mussgiller, A. Nürnberg, Y. Otarid, D. Pérez Adán, A. Raspereza, B. Ribeiro Lopes, J. Rübenach, A. Saggio, A. Saibel, M. Savitskyi, M. Scham [25,22], V. Scheurer, S. Schnake [22], P. Schütze, C. Schwanenberger [21], M. Shchedrolosiev, R.E. Sosa Ricardo, D. Stafford, N. Tonon [†], M. Van De Klundert, F. Vazzoler, A. Ventura Barroso, R. Walsh, D. Walter, Q. Wang, Y. Wen, K. Wichmann, L. Wiens [22], C. Wissing, S. Wuchterl, Y. Yang, A. Zimermmane Castro Santos

Deutsches Elektronen-Synchrotron, Hamburg, Germany

R. Aggleton, A. Albrecht, S. Albrecht, M. Antonello, S. Bein, L. Benato, M. Bonanomi, P. Connor, K. De Leo, M. Eich, K. El Morabit, F. Feindt, A. Fröhlich, C. Garbers, E. Garutti, M. Hajheidari, J. Haller, A. Hinzmann, H.R. Jabusch, G. Kasieczka, R. Klanner, W. Korcari, T. Kramer, V. Kutzner, J. Lange, T. Lange, A. Lobanov, C. Matthies, A. Mehta, L. Moureaux, M. Mrowietz, A. Nigamova, Y. Nissan, A. Paasch, K.J. Pena Rodriguez, M. Rieger, O. Rieger, P. Schleper, M. Schröder, J. Schwandt, H. Stadie, G. Steinbrück, A. Tews, M. Wolf

University of Hamburg, Hamburg, Germany

J. Bechtel, S. Brommer, M. Burkart, E. Butz, R. Caspart, T. Chwalek, A. Dierlamm, A. Droll, N. Faltermann, M. Giffels, J.O. Gosewisch, A. Gottmann, F. Hartmann [20], C. Heidecker, M. Horzela, U. Husemann, P. Keicher, M. Klute, R. Koppenhöfer, S. Maier, S. Mitra, Th. Müller, M. Neukum, G. Quast, K. Rabbertz, J. Rauser, D. Savoiu, M. Schnepf, D. Seith, I. Shvetsov, H.J. Simonis, N. Trevisani, R. Ulrich, J. van der Linden, R.F. Von Cube, M. Wassmer, M. Weber, S. Wieland, R. Wolf, S. Wozniewski, S. Wunsch

Karlsruher Institut fuer Technologie, Karlsruhe, Germany

G. Anagnostou, P. Assiouras, G. Daskalakis, A. Kyriakis, A. Stakia

Institute of Nuclear and Particle Physics (INPP), NCSR Demokritos, Aghia Paraskevi, Greece

M. Diamantopoulou, D. Karasavvas, P. Kontaxakis, A. Manousakis-Katsikakis, A. Panagiotou, I. Papavergou, N. Saoulidou, K. Theofilatos, E. Tziaferi, K. Vellidis, E. Vourliotis

National and Kapodistrian University of Athens, Athens, Greece

G. Bakas, T. Chatzistavrou, K. Kousouris, I. Papakrivopoulos, G. Tsipolitis, A. Zacharopoulou

National Technical University of Athens, Athens, Greece

K. Adamidis, I. Bestintzanos, I. Evangelou, C. Foudas, P. Gianneios, C. Kamtsikis, P. Katsoulis, P. Kokkas, P.G. Kosmoglou Kioseoglou, N. Manthos, I. Papadopoulos, J. Strologas

University of Ioánnina, Ioánnina, Greece

M. Csanád, K. Farkas, M.M.A. Gadallah [26], S. Lökös [27], P. Major, K. Mandal, G. Pásztor, A.J. Rádl [28], O. Surányi, G.I. Veres

MTA-ELTE Lendület CMS Particle and Nuclear Physics Group, Eötvös Loránd University, Budapest, Hungary

M. Bartók [29], G. Bencze, C. Hajdu, D. Horvath [30,31], F. Sikler, V. Veszpremi

Wigner Research Centre for Physics, Budapest, Hungary

N. Beni, S. Czellar, D. Fasanella, J. Karancsi [29], J. Molnar, Z. Szillasi, D. Teyssier

Institute of Nuclear Research ATOMKI, Debrecen, Hungary

P. Raics, B. Ujvari [32]

Institute of Physics, University of Debrecen, Debrecen, Hungary

T. Csorgo [28], F. Nemes [28], T. Novak

Karoly Robert Campus, MATE Institute of Technology, Gyongyos, Hungary

J. Babbar, S. Bansal, S.B. Beri, V. Bhatnagar, G. Chaudhary, S. Chauhan, N. Dhingra [33], R. Gupta, A. Kaur, A. Kaur, H. Kaur, M. Kaur, S. Kumar, P. Kumari, M. Meena, K. Sandeep, T. Sheokand, J.B. Singh [34], A. Singla, A.K. Virdi

Panjab University, Chandigarh, India

A. Ahmed, A. Bhardwaj, B.C. Choudhary, M. Gola, S. Keshri, A. Kumar, M. Naimuddin, P. Priyanka, K. Ranjan, S. Saumya, A. Shah

University of Delhi, Delhi, India

S. Baradia, S. Barman [35], S. Bhattacharya, D. Bhowmik, S. Dutta, S. Dutta, B. Gomber [36], M. Maity [35], P. Palit, P.K. Rout, G. Saha, B. Sahu, S. Sarkar

Saha Institute of Nuclear Physics, HBNI, Kolkata, India

P.K. Behera, S.C. Behera, P. Kalbhor, J.R. Komaragiri [37], D. Kumar [37], A. Muhammad, L. Panwar [37], R. Pradhan, P.R. Pujahari, A. Sharma, A.K. Sikdar, P.C. Tiwari [37], S. Verma

Indian Institute of Technology Madras, Madras, India

K. Naskar [38]

Bhabha Atomic Research Centre, Mumbai, India

T. Aziz, I. Das, S. Dugad, M. Kumar, G.B. Mohanty, P. Suryadevara

Tata Institute of Fundamental Research-A, Mumbai, India

S. Banerjee, R. Chudasama, M. Guchait, S. Karmakar, S. Kumar, G. Majumder, K. Mazumdar, S. Mukherjee, A. Thachayath

Tata Institute of Fundamental Research-B, Mumbai, India

S. Bahinipati [39], A.K. Das, C. Kar, P. Mal, T. Mishra, V.K. Muraleedharan Nair Bindhu [40], A. Nayak [40], P. Saha, N. Sur, S.K. Swain, D. Vats [40]

National Institute of Science Education and Research, An OCC of Homi Bhabha National Institute, Bhubaneswar, Odisha, India

A. Alpana, S. Dube, B. Kansal, A. Laha, S. Pandey, A. Rastogi, S. Sharma

Indian Institute of Science Education and Research (IISER), Pune, India

H. Bakhshiansohi [41], E. Khazaie, M. Zeinali [42]

Isfahan University of Technology, Isfahan, Iran

S. Chenarani [43], S.M. Etesami, M. Khakzad, M. Mohammadi Najafabadi

Institute for Research in Fundamental Sciences (IPM), Tehran, Iran

M. Grunewald

University College Dublin, Dublin, Ireland

M. Abbrescia [a,b], R. Aly [a,c,44], C. Aruta [a,b], A. Colaleo [a], D. Creanza [a,c], N. De Filippis [a,c], M. De Palma [a,b], A. Di Florio [a,b], W. Elmetenawee [a,b], F. Errico [a,b], L. Fiore [a], G. Iaselli [a,c], M. Ince [a,b], G. Maggi [a,c], M. Maggi [a], I. Margjeka [a,b], V. Mastrapasqua [a,b], S. My [a,b], S. Nuzzo [a,b], A. Pellecchia [a,b], A. Pompili [a,b], G. Pugliese [a,c], R. Radogna [a], D. Ramos [a], A. Ranieri [a], G. Selvaggi [a,b], L. Silvestris [a], F.M. Simone [a,b], Ü. Sözbilir [a], A. Stamerra [a], R. Venditti [a], P. Verwilligen [a], A. Zaza [a,b]

[a] *INFN Sezione di Bari, Bari, Italy*
[b] *Università di Bari, Bari, Italy*
[c] *Politecnico di Bari, Bari, Italy*

G. Abbiendi [a], C. Battilana [a,b], D. Bonacorsi [a,b], L. Borgonovi [a], L. Brigliadori [a], R. Campanini [a,b], P. Capiluppi [a,b], A. Castro [a,b], F.R. Cavallo [a], M. Cuffiani [a,b], G.M. Dallavalle [a], T. Diotalevi [a,b], F. Fabbri [a], A. Fanfani [a,b], P. Giacomelli [a], L. Giommi [a,b], C. Grandi [a], L. Guiducci [a,b], S. Lo Meo [a,45], L. Lunerti [a,b], S. Marcellini [a], G. Masetti [a], F.L. Navarria [a,b], A. Perrotta [a], F. Primavera [a,b], A.M. Rossi [a,b], T. Rovelli [a,b], G.P. Siroli [a,b]

[a] *INFN Sezione di Bologna, Bologna, Italy*
[b] *Università di Bologna, Bologna, Italy*

S. Costa [a,b,46], A. Di Mattia [a], R. Potenza [a,b], A. Tricomi [a,b,46], C. Tuve [a,b]

[a] *INFN Sezione di Catania, Catania, Italy*
[b] *Università di Catania, Catania, Italy*

G. Barbagli [a], B. Camaiani [a,b], A. Cassese [a], R. Ceccarelli [a,b], V. Ciulli [a,b], C. Civinini [a], R. D'Alessandro [a,b], E. Focardi [a,b], G. Latino [a,b], P. Lenzi [a,b], M. Lizzo [a,b], M. Meschini [a], S. Paoletti [a], R. Seidita [a,b], G. Sguazzoni [a], L. Viliani [a]

[a] *INFN Sezione di Firenze, Firenze, Italy*
[b] *Università di Firenze, Firenze, Italy*

L. Benussi, S. Bianco, S. Meola [20], D. Piccolo

INFN Laboratori Nazionali di Frascati, Frascati, Italy

M. Bozzo [a,b], F. Ferro [a], R. Mulargia [a], E. Robutti [a], S. Tosi [a,b]

[a] *INFN Sezione di Genova, Genova, Italy*
[b] *Università di Genova, Genova, Italy*

A. Benaglia [a], G. Boldrini [a], F. Brivio [a,b], F. Cetorelli [a,b], F. De Guio [a,b], M.E. Dinardo [a,b], P. Dini [a], S. Gennai [a], A. Ghezzi [a,b], P. Govoni [a,b], L. Guzzi [a,b], M.T. Lucchini [a,b], M. Malberti [a], S. Malvezzi [a], A. Massironi [a], D. Menasce [a], L. Moroni [a], M. Paganoni [a,b], D. Pedrini [a], B.S. Pinolini [a], S. Ragazzi [a,b], N. Redaelli [a], T. Tabarelli de Fatis [a,b], D. Zuolo [a,b]

[a] *INFN Sezione di Milano-Bicocca, Milano, Italy*
[b] *Università di Milano-Bicocca, Milano, Italy*

S. Buontempo [a], F. Carnevali [a,b], N. Cavallo [a,c], A. De Iorio [a,b], F. Fabozzi [a,c], A.O.M. Iorio [a,b], L. Lista [a,b,47], P. Paolucci [a,20], B. Rossi [a], C. Sciacca [a,b]

[a] *INFN Sezione di Napoli, Napoli, Italy*

[b] Università di Napoli 'Federico II', Napoli, Italy
[c] Università della Basilicata, Potenza, Italy
[d] Università G. Marconi, Roma, Italy

P. Azzi [a], N. Bacchetta [a,48], D. Bisello [a,b], P. Bortignon [a], A. Bragagnolo [a,b], R. Carlin [a,b], P. Checchia [a], T. Dorigo [a], F. Gasparini [a,b], U. Gasparini [a,b], G. Grosso [a], L. Layer [a,49], E. Lusiani [a], M. Margoni [a,b], A.T. Meneguzzo [a,b], J. Pazzini [a,b], P. Ronchese [a,b], R. Rossin [a,b], F. Simonetto [a,b], G. Strong [a], M. Tosi [a,b], H. Yarar [a,b], M. Zanetti [a,b], P. Zotto [a,b], A. Zucchetta [a,b], G. Zumerle [a,b]

[a] INFN Sezione di Padova, Padova, Italy
[b] Università di Padova, Padova, Italy
[c] Università di Trento, Trento, Italy

C. Aimè [a,b], A. Braghieri [a], S. Calzaferri [a,b], D. Fiorina [a,b], P. Montagna [a,b], V. Re [a], C. Riccardi [a,b], P. Salvini [a], I. Vai [a], P. Vitulo [a,b]

[a] INFN Sezione di Pavia, Pavia, Italy
[b] Università di Pavia, Pavia, Italy

P. Asenov [a,50], G.M. Bilei [a], D. Ciangottini [a,b], L. Fanò [a,b], M. Magherini [a,b], G. Mantovani [a,b], V. Mariani [a,b], M. Menichelli [a], F. Moscatelli [a,50], A. Piccinelli [a,b], M. Presilla [a,b], A. Rossi [a,b], A. Santocchia [a,b], D. Spiga [a], T. Tedeschi [a,b]

[a] INFN Sezione di Perugia, Perugia, Italy
[b] Università di Perugia, Perugia, Italy

P. Azzurri [a], G. Bagliesi [a], V. Bertacchi [a,c], R. Bhattacharya [a], L. Bianchini [a,b], T. Boccali [a], E. Bossini [a,b], D. Bruschini [a,c], R. Castaldi [a], M.A. Ciocci [a,b], V. D'Amante [a,d], R. Dell'Orso [a], M.R. Di Domenico [a,d], S. Donato [a], A. Giassi [a], M.T. Grippo [a,d], F. Ligabue [a,c], E. Manca [a,c], G. Mandorli [a,c], D. Matos Figueiredo [a], A. Messineo [a,b], M. Musich [a,b], F. Palla [a], S. Parolia [a,b], G. Ramirez-Sanchez [a,c], A. Rizzi [a,b], G. Rolandi [a,c], S. Roy Chowdhury [a,c], A. Scribano [a], N. Shafiei [a,b], P. Spagnolo [a], R. Tenchini [a], G. Tonelli [a,b], N. Turini [a,d], A. Venturi [a], P.G. Verdini [a]

[a] INFN Sezione di Pisa, Pisa, Italy
[b] Università di Pisa, Pisa, Italy
[c] Scuola Normale Superiore di Pisa, Pisa, Italy
[d] Università di Siena, Siena, Italy

P. Barria [a], M. Campana [a,b], F. Cavallari [a], D. Del Re [a,b], E. Di Marco [a], M. Diemoz [a], E. Longo [a,b], P. Meridiani [a], G. Organtini [a,b], F. Pandolfi [a], R. Paramatti [a,b], C. Quaranta [a,b], S. Rahatlou [a,b], C. Rovelli [a], F. Santanastasio [a,b], L. Soffi [a], R. Tramontano [a,b]

[a] INFN Sezione di Roma, Roma, Italy
[b] Sapienza Università di Roma, Roma, Italy

N. Amapane [a,b], R. Arcidiacono [a,c], S. Argiro [a,b], M. Arneodo [a,c], N. Bartosik [a], R. Bellan [a,b], A. Bellora [a,b], J. Berenguer Antequera [a,b], C. Biino [a], N. Cartiglia [a], M. Costa [a,b], R. Covarelli [a,b], N. Demaria [a], M. Grippo [a,b], B. Kiani [a,b], F. Legger [a], C. Mariotti [a], S. Maselli [a], A. Mecca [a,b], E. Migliore [a,b], E. Monteil [a,b], M. Monteno [a], M.M. Obertino [a,b], G. Ortona [a], L. Pacher [a,b], N. Pastrone [a], M. Pelliccioni [a], M. Ruspa [a,c], K. Shchelina [a], F. Siviero [a,b], V. Sola [a], A. Solano [a,b], D. Soldi [a,b], A. Staiano [a], M. Tornago [a,b], D. Trocino [a], G. Umoret [a,b], A. Vagnerini [a,b]

[a] INFN Sezione di Torino, Torino, Italy
[b] Università di Torino, Torino, Italy
[c] Università del Piemonte Orientale, Novara, Italy

S. Belforte [a], V. Candelise [a,b], M. Casarsa [a], F. Cossutti [a], A. Da Rold [a,b], G. Della Ricca [a,b], G. Sorrentino [a,b]

[a] INFN Sezione di Trieste, Trieste, Italy
[b] Università di Trieste, Trieste, Italy

S. Dogra, C. Huh, B. Kim, D.H. Kim, G.N. Kim, J. Kim, J. Lee, S.W. Lee, C.S. Moon, Y.D. Oh, S.I. Pak, S. Sekmen, Y.C. Yang

Kyungpook National University, Daegu, Korea

H. Kim, D.H. Moon

Chonnam National University, Institute for Universe and Elementary Particles, Kwangju, Korea

E. Asilar, T.J. Kim, J. Park

Hanyang University, Seoul, Korea

S. Cho, S. Choi, S. Han, B. Hong, K. Lee, K.S. Lee, J. Lim, J. Park, S.K. Park, J. Yoo

Korea University, Seoul, Korea

J. Goh

Kyung Hee University, Department of Physics, Seoul, Korea

H.S. Kim, Y. Kim, S. Lee

Sejong University, Seoul, Korea

J. Almond, J.H. Bhyun, J. Choi, S. Jeon, W. Jun, J. Kim, J. Kim, J.S. Kim, S. Ko, H. Kwon, H. Lee, J. Lee, S. Lee, B.H. Oh, M. Oh, S.B. Oh, H. Seo, U.K. Yang, I. Yoon

Seoul National University, Seoul, Korea

W. Jang, D.Y. Kang, Y. Kang, D. Kim, S. Kim, B. Ko, J.S.H. Lee, Y. Lee, J.A. Merlin, I.C. Park, Y. Roh, M.S. Ryu, D. Song, I.J. Watson, S. Yang

University of Seoul, Seoul, Korea

S. Ha, H.D. Yoo

Yonsei University, Department of Physics, Seoul, Korea

M. Choi, H. Lee, Y. Lee, I. Yu

Sungkyunkwan University, Suwon, Korea

T. Beyrouthy, Y. Maghrbi

College of Engineering and Technology, American University of the Middle East (AUM), Dasman, Kuwait

K. Dreimanis, A. Gaile, A. Potrebko, T. Torims, V. Veckalns

Riga Technical University, Riga, Latvia

M. Ambrozas, A. Carvalho Antunes De Oliveira, A. Juodagalvis, A. Rinkevicius, G. Tamulaitis

Vilnius University, Vilnius, Lithuania

N. Bin Norjoharuddeen, S.Y. Hoh [51], I. Yusuff [51], Z. Zolkapli

National Centre for Particle Physics, Universiti Malaya, Kuala Lumpur, Malaysia

J.F. Benitez, A. Castaneda Hernandez, H.A. Encinas Acosta, L.G. Gallegos Maríñez, M. León Coello, J.A. Murillo Quijada, A. Sehrawat, L. Valencia Palomo

Universidad de Sonora (UNISON), Hermosillo, Mexico

G. Ayala, H. Castilla-Valdez, E. De La Cruz-Burelo, I. Heredia-De La Cruz [52], R. Lopez-Fernandez, C.A. Mondragon Herrera, D.A. Perez Navarro, A. Sánchez Hernández

Centro de Investigacion y de Estudios Avanzados del IPN, Mexico City, Mexico

C. Oropeza Barrera, F. Vazquez Valencia

Universidad Iberoamericana, Mexico City, Mexico

I. Pedraza, H.A. Salazar Ibarguen, C. Uribe Estrada

Benemerita Universidad Autonoma de Puebla, Puebla, Mexico

I. Bubanja, J. Mijuskovic [53], N. Raicevic

University of Montenegro, Podgorica, Montenegro

A. Ahmad, M.I. Asghar, A. Awais, M.I.M. Awan, M. Gul, H.R. Hoorani, W.A. Khan, M. Shoaib, M. Waqas

National Centre for Physics, Quaid-I-Azam University, Islamabad, Pakistan

V. Avati, L. Grzanka, M. Malawski

AGH University of Science and Technology Faculty of Computer Science, Electronics and Telecommunications, Krakow, Poland

H. Bialkowska, M. Bluj, B. Boimska, M. Górski, M. Kazana, M. Szleper, P. Zalewski

National Centre for Nuclear Research, Swierk, Poland

K. Bunkowski, K. Doroba, A. Kalinowski, M. Konecki, J. Krolikowski

Institute of Experimental Physics, Faculty of Physics, University of Warsaw, Warsaw, Poland

M. Araujo, P. Bargassa, D. Bastos, A. Boletti, P. Faccioli, M. Gallinaro, J. Hollar, N. Leonardo, T. Niknejad, M. Pisano, J. Seixas, O. Toldaiev, J. Varela

Laboratório de Instrumentação e Física Experimental de Partículas, Lisboa, Portugal

P. Adzic [54], M. Dordevic, P. Milenovic, J. Milosevic

VINCA Institute of Nuclear Sciences, University of Belgrade, Belgrade, Serbia

M. Aguilar-Benitez, J. Alcaraz Maestre, A. Álvarez Fernández, M. Barrio Luna, Cristina F. Bedoya, C.A. Carrillo Montoya, M. Cepeda, M. Cerrada, N. Colino, B. De La Cruz, A. Delgado Peris, D. Fernández Del Val, J.P. Fernández Ramos, J. Flix, M.C. Fouz, O. Gonzalez Lopez, S. Goy Lopez, J.M. Hernandez, M.I. Josa, J. León Holgado, D. Moran, C. Perez Dengra, A. Pérez-Calero Yzquierdo, J. Puerta Pelayo, I. Redondo, D.D. Redondo Ferrero, L. Romero, S. Sánchez Navas, J. Sastre, L. Urda Gómez, J. Vazquez Escobar, C. Willmott

Centro de Investigaciones Energéticas Medioambientales y Tecnológicas (CIEMAT), Madrid, Spain

J.F. de Trocóniz

Universidad Autónoma de Madrid, Madrid, Spain

B. Alvarez Gonzalez, J. Cuevas, J. Fernandez Menendez, S. Folgueras, I. Gonzalez Caballero, J.R. González Fernández, E. Palencia Cortezon, C. Ramón Álvarez, V. Rodríguez Bouza, A. Soto Rodríguez, A. Trapote, C. Vico Villalba

Universidad de Oviedo, Instituto Universitario de Ciencias y Tecnologías Espaciales de Asturias (ICTEA), Oviedo, Spain

J.A. Brochero Cifuentes, I.J. Cabrillo, A. Calderon, J. Duarte Campderros, M. Fernandez, C. Fernandez Madrazo, A. García Alonso, G. Gomez, C. Lasaosa García, C. Martinez Rivero, P. Martinez Ruiz del Arbol, F. Matorras, P. Matorras Cuevas, J. Piedra Gomez, C. Prieels, A. Ruiz-Jimeno, L. Scodellaro, I. Vila, J.M. Vizan Garcia

Instituto de Física de Cantabria (IFCA), CSIC-Universidad de Cantabria, Santander, Spain

M.K. Jayananda, B. Kailasapathy [55], D.U.J. Sonnadara, D.D.C. Wickramarathna

University of Colombo, Colombo, Sri Lanka

W.G.D. Dharmaratna, K. Liyanage, N. Perera, N. Wickramage

University of Ruhuna, Department of Physics, Matara, Sri Lanka

D. Abbaneo, J. Alimena, E. Auffray, G. Auzinger, J. Baechler, P. Baillon [†], D. Barney, J. Bendavid, M. Bianco, B. Bilin, A. Bocci, E. Brondolin, C. Caillol, T. Camporesi, G. Cerminara, N. Chernyavskaya, S.S. Chhibra, S. Choudhury, M. Cipriani, L. Cristella, D. d'Enterria, A. Dabrowski, A. David, A. De Roeck, M.M. Defranchis, M. Deile, M. Dobson, M. Dünser, N. Dupont, A. Elliott-Peisert, F. Fallavollita [56], A. Florent, L. Forthomme, G. Franzoni, W. Funk, S. Ghosh, S. Giani, D. Gigi, K. Gill, F. Glege, L. Gouskos, E. Govorkova, M. Haranko, J. Hegeman, V. Innocente, T. James, P. Janot, J. Kaspar, J. Kieseler, N. Kratochwil, S. Laurila, P. Lecoq, A. Lintuluoto, C. Lourenço, B. Maier, L. Malgeri, M. Mannelli, A.C. Marini, F. Meijers, S. Mersi, E. Meschi, F. Moortgat, M. Mulders, S. Orfanelli, L. Orsini, F. Pantaleo, E. Perez, M. Peruzzi, A. Petrilli, G. Petrucciani, A. Pfeiffer, M. Pierini, D. Piparo, M. Pitt, H. Qu, T. Quast, D. Rabady, A. Racz, G. Reales Gutiérrez, M. Rovere, H. Sakulin, J. Salfeld-Nebgen, S. Scarfi, M. Selvaggi, A. Sharma, P. Silva, P. Sphicas [57], A.G. Stahl Leiton, S. Summers, K. Tatar, V.R. Tavolaro, D. Treille, P. Tropea, A. Tsirou, J. Wanczyk [58], K.A. Wozniak, W.D. Zeuner

CERN, European Organization for Nuclear Research, Geneva, Switzerland

L. Caminada [59], A. Ebrahimi, W. Erdmann, R. Horisberger, Q. Ingram, H.C. Kaestli, D. Kotlinski, C. Lange, M. Missiroli [59], L. Noehte [59], T. Rohe

Paul Scherrer Institut, Villigen, Switzerland

T.K. Aarrestad, K. Androsov [58], M. Backhaus, P. Berger, A. Calandri, A. De Cosa, G. Dissertori, M. Dittmar, M. Donegà, F. Eble, M. Galli, K. Gedia, F. Glessgen, T.A. Gómez Espinosa, C. Grab, D. Hits, W. Lustermann, A.-M. Lyon, R.A. Manzoni, L. Marchese, C. Martin Perez, A. Mascellani [58], M.T. Meinhard, F. Nessi-Tedaldi, J. Niedziela, F. Pauss, V. Perovic, S. Pigazzini, M.G. Ratti, M. Reichmann, C. Reissel, T. Reitenspiess, B. Ristic, F. Riti, D. Ruini, D.A. Sanz Becerra, J. Steggemann [58], D. Valsecchi [20], R. Wallny

ETH Zurich – Institute for Particle Physics and Astrophysics (IPA), Zurich, Switzerland

C. Amsler [60], P. Bärtschi, C. Botta, D. Brzhechko, M.F. Canelli, K. Cormier, A. De Wit, R. Del Burgo, J.K. Heikkilä, M. Huwiler, W. Jin, A. Jofrehei, B. Kilminster, S. Leontsinis, S.P. Liechti, A. Macchiolo, P. Meiring, V.M. Mikuni, U. Molinatti, I. Neutelings, A. Reimers, P. Robmann, S. Sanchez Cruz, K. Schweiger, M. Senger, Y. Takahashi

Universität Zürich, Zurich, Switzerland

C. Adloff [61], C.M. Kuo, W. Lin, S.S. Yu

National Central University, Chung-Li, Taiwan

L. Ceard, Y. Chao, K.F. Chen, P.s. Chen, H. Cheng, W.-S. Hou, Y.y. Li, R.-S. Lu, E. Paganis, A. Psallidas, A. Steen, H.y. Wu, E. Yazgan, P.r. Yu

National Taiwan University (NTU), Taipei, Taiwan

C. Asawatangtrakuldee, N. Srimanobhas

Chulalongkorn University, Faculty of Science, Department of Physics, Bangkok, Thailand

D. Agyel, F. Boran, Z.S. Demiroglu, F. Dolek, I. Dumanoglu [62], E. Eskut, Y. Guler [63], E. Gurpinar Guler [63], C. Isik, O. Kara, A. Kayis Topaksu, U. Kiminsu, G. Onengut, K. Ozdemir [64], A. Polatoz, A.E. Simsek, B. Tali [65], U.G. Tok, S. Turkcapar, E. Uslan, I.S. Zorbakir

Çukurova University, Physics Department, Science and Art Faculty, Adana, Turkey

G. Karapinar, K. Ocalan [66], M. Yalvac [67]

Middle East Technical University, Physics Department, Ankara, Turkey

B. Akgun, I.O. Atakisi, E. Gülmez, M. Kaya [68], O. Kaya [69], Ö. Özçelik, S. Tekten [70]

Bogazici University, Istanbul, Turkey

A. Cakir, K. Cankocak [62], Y. Komurcu, S. Sen [71]

Istanbul Technical University, Istanbul, Turkey

O. Aydilek, S. Cerci [65], B. Hacisahinoglu, I. Hos [72], B. Isildak [73], B. Kaynak, S. Ozkorucuklu, C. Simsek, D. Sunar Cerci [65]

Istanbul University, Istanbul, Turkey

B. Grynyov

Institute for Scintillation Materials of National Academy of Science of Ukraine, Kharkiv, Ukraine

L. Levchuk

National Science Centre, Kharkiv Institute of Physics and Technology, Kharkiv, Ukraine

D. Anthony, E. Bhal, J.J. Brooke, A. Bundock, E. Clement, D. Cussans, H. Flacher, M. Glowacki, J. Goldstein, G.P. Heath, H.F. Heath, L. Kreczko, B. Krikler, S. Paramesvaran, S. Seif El Nasr-Storey, V.J. Smith, N. Stylianou [74], K. Walkingshaw Pass, R. White

University of Bristol, Bristol, United Kingdom

A.H. Ball, K.W. Bell, A. Belyaev [75], C. Brew, R.M. Brown, D.J.A. Cockerill, C. Cooke, K.V. Ellis, K. Harder, S. Harper, M.-L. Holmberg [76], J. Linacre, K. Manolopoulos, D.M. Newbold, E. Olaiya, D. Petyt, T. Reis, G. Salvi, T. Schuh, C.H. Shepherd-Themistocleous, I.R. Tomalin, T. Williams

Rutherford Appleton Laboratory, Didcot, United Kingdom

R. Bainbridge, P. Bloch, S. Bonomally, J. Borg, S. Breeze, C.E. Brown, O. Buchmuller, V. Cacchio, V. Cepaitis, G.S. Chahal [77], D. Colling, J.S. Dancu, P. Dauncey, G. Davies, J. Davies, M. Della Negra, S. Fayer, G. Fedi, G. Hall, M.H. Hassanshahi, A. Howard, G. Iles, J. Langford, L. Lyons, A.-M. Magnan, S. Malik, A. Martelli, M. Mieskolainen, D.G. Monk, J. Nash [78], M. Pesaresi, B.C. Radburn-Smith, D.M. Raymond, A. Richards, A. Rose, E. Scott, C. Seez, A. Shtipliyski, R. Shukla, A. Tapper, K. Uchida, G.P. Uttley, L.H. Vage, T. Virdee [20], M. Vojinovic, N. Wardle, S.N. Webb, D. Winterbottom

Imperial College, London, United Kingdom

K. Coldham, J.E. Cole, A. Khan, P. Kyberd, I.D. Reid, L. Teodorescu, S. Zahid

Brunel University, Uxbridge, United Kingdom

S. Abdullin, A. Brinkerhoff, B. Caraway, J. Dittmann, K. Hatakeyama, A.R. Kanuganti, B. McMaster, M. Saunders, S. Sawant, C. Sutantawibul, J. Wilson

Baylor University, Waco, TX, USA

R. Bartek, A. Dominguez, R. Uniyal, A.M. Vargas Hernandez

Catholic University of America, Washington, DC, USA

A. Buccilli, S.I. Cooper, D. Di Croce, S.V. Gleyzer, C. Henderson, C.U. Perez, P. Rumerio [79], C. West

The University of Alabama, Tuscaloosa, AL, USA

A. Akpinar, A. Albert, D. Arcaro, C. Cosby, Z. Demiragli, C. Erice, E. Fontanesi, D. Gastler, S. May, J. Rohlf, K. Salyer, D. Sperka, D. Spitzbart, I. Suarez, A. Tsatsos, S. Yuan

Boston University, Boston, MA, USA

G. Benelli, B. Burkle, X. Coubez [22], D. Cutts, M. Hadley, U. Heintz, J.M. Hogan [80], T. Kwon, G. Landsberg, K.T. Lau, D. Li, J. Luo, M. Narain, N. Pervan, S. Sagir [81], F. Simpson, E. Usai, W.Y. Wong, X. Yan, D. Yu, W. Zhang

Brown University, Providence, RI, USA

J. Bonilla, C. Brainerd, R. Breedon, M. Calderon De La Barca Sanchez, M. Chertok, J. Conway, P.T. Cox, R. Erbacher, G. Haza, F. Jensen, O. Kukral, G. Mocellin, M. Mulhearn, D. Pellett, B. Regnery, D. Taylor, Y. Yao, F. Zhang

University of California, Davis, Davis, CA, USA

M. Bachtis, R. Cousins, A. Datta, D. Hamilton, J. Hauser, M. Ignatenko, M.A. Iqbal, T. Lam, W.A. Nash, S. Regnard, D. Saltzberg, B. Stone, V. Valuev

University of California, Los Angeles, CA, USA

Y. Chen, R. Clare, J.W. Gary, M. Gordon, G. Hanson, G. Karapostoli, O.R. Long, N. Manganelli, W. Si, S. Wimpenny

University of California, Riverside, Riverside, CA, USA

J.G. Branson, P. Chang, S. Cittolin, S. Cooperstein, D. Diaz, J. Duarte, R. Gerosa, L. Giannini, J. Guiang, R. Kansal, V. Krutelyov, R. Lee, J. Letts, M. Masciovecchio, F. Mokhtar, M. Pieri, B.V. Sathia Narayanan, V. Sharma, M. Tadel, F. Würthwein, Y. Xiang, A. Yagil

University of California, San Diego, La Jolla, CA, USA

N. Amin, C. Campagnari, M. Citron, G. Collura, A. Dorsett, V. Dutta, J. Incandela, M. Kilpatrick, J. Kim, A.J. Li, B. Marsh, P. Masterson, H. Mei, M. Oshiro, M. Quinnan, J. Richman, U. Sarica, R. Schmitz, F. Setti, J. Sheplock, P. Siddireddy, D. Stuart, S. Wang

University of California, Santa Barbara – Department of Physics, Santa Barbara, CA, USA

A. Bornheim, O. Cerri, I. Dutta, J.M. Lawhorn, N. Lu, J. Mao, H.B. Newman, T.Q. Nguyen, M. Spiropulu, J.R. Vlimant, C. Wang, S. Xie, Z. Zhang, R.Y. Zhu

California Institute of Technology, Pasadena, CA, USA

J. Alison, S. An, M.B. Andrews, P. Bryant, T. Ferguson, A. Harilal, C. Liu, T. Mudholkar, S. Murthy, M. Paulini, A. Roberts, A. Sanchez, W. Terrill

Carnegie Mellon University, Pittsburgh, PA, USA

J.P. Cumalat, W.T. Ford, A. Hassani, G. Karathanasis, E. MacDonald, F. Marini, R. Patel, A. Perloff, C. Savard, N. Schonbeck, K. Stenson, K.A. Ulmer, S.R. Wagner, N. Zipper

University of Colorado Boulder, Boulder, CO, USA

J. Alexander, S. Bright-Thonney, X. Chen, D.J. Cranshaw, J. Fan, X. Fan, D. Gadkari, S. Hogan, J. Monroy, J.R. Patterson, D. Quach, J. Reichert, M. Reid, A. Ryd, J. Thom, P. Wittich, R. Zou

Cornell University, Ithaca, NY, USA

M. Albrow, M. Alyari, G. Apollinari, A. Apresyan, L.A.T. Bauerdick, D. Berry, J. Berryhill, P.C. Bhat, K. Burkett, J.N. Butler, A. Canepa, G.B. Cerati, H.W.K. Cheung, F. Chlebana, K.F. Di Petrillo, J. Dickinson, V.D. Elvira, Y. Feng, J. Freeman, A. Gandrakota, Z. Gecse, L. Gray, D. Green, S. Grünendahl, O. Gutsche, R.M. Harris, R. Heller, T.C. Herwig, J. Hirschauer, L. Horyn, B. Jayatilaka, S. Jindariani, M. Johnson, U. Joshi, T. Klijnsma, B. Klima, K.H.M. Kwok, S. Lammel, D. Lincoln, R. Lipton, T. Liu, C. Madrid, K. Maeshima, C. Mantilla, D. Mason, P. McBride, P. Merkel, S. Mrenna, S. Nahn, J. Ngadiuba, V. Papadimitriou, N. Pastika, K. Pedro, C. Pena [82], F. Ravera, A. Reinsvold Hall [83], L. Ristori, E. Sexton-Kennedy, N. Smith, A. Soha, L. Spiegel, J. Strait, L. Taylor, S. Tkaczyk, N.V. Tran, L. Uplegger, E.W. Vaandering, H.A. Weber, I. Zoi

Fermi National Accelerator Laboratory, Batavia, IL, USA

P. Avery, D. Bourilkov, L. Cadamuro, V. Cherepanov, R.D. Field, D. Guerrero, M. Kim, E. Koenig, J. Konigsberg, A. Korytov, K.H. Lo, K. Matchev, N. Menendez, G. Mitselmakher, A. Muthirakalayil Madhu, N. Rawal, D. Rosenzweig, S. Rosenzweig, K. Shi, J. Wang, Z. Wu

University of Florida, Gainesville, FL, USA

T. Adams, A. Askew, R. Habibullah, V. Hagopian, R. Khurana, T. Kolberg, G. Martinez, H. Prosper, C. Schiber, O. Viazlo, R. Yohay, J. Zhang

Florida State University, Tallahassee, FL, USA

M.M. Baarmand, S. Butalla, T. Elkafrawy [84], M. Hohlmann, R. Kumar Verma, D. Noonan, M. Rahmani, F. Yumiceva

Florida Institute of Technology, Melbourne, FL, USA

M.R. Adams, H. Becerril Gonzalez, R. Cavanaugh, S. Dittmer, O. Evdokimov, C.E. Gerber, D.J. Hofman, D.S. Lemos, A.H. Merrit, C. Mills, G. Oh, T. Roy, S. Rudrabhatla, M.B. Tonjes, N. Varelas, X. Wang, Z. Ye, J. Yoo

University of Illinois at Chicago (UIC), Chicago, IL, USA

M. Alhusseini, K. Dilsiz [85], L. Emediato, R.P. Gandrajula, G. Karaman, O.K. Köseyan, J.-P. Merlo, A. Mestvirishvili [86], J. Nachtman, O. Neogi, H. Ogul [87], Y. Onel, A. Penzo, C. Snyder, E. Tiras [88]

The University of Iowa, Iowa City, IA, USA

O. Amram, B. Blumenfeld, L. Corcodilos, J. Davis, A.V. Gritsan, L. Kang, S. Kyriacou, P. Maksimovic, J. Roskes, S. Sekhar, M. Swartz, T.Á. Vámi

Johns Hopkins University, Baltimore, MD, USA

A. Abreu, L.F. Alcerro Alcerro, J. Anguiano, P. Baringer, A. Bean, Z. Flowers, T. Isidori, S. Khalil, J. King, G. Krintiras, M. Lazarovits, C. Le Mahieu, C. Lindsey, J. Marquez, N. Minafra, M. Murray, M. Nickel, C. Rogan, C. Royon, R. Salvatico, S. Sanders, E. Schmitz, C. Smith, Q. Wang, Z. Warner, J. Williams, G. Wilson

The University of Kansas, Lawrence, KS, USA

B. Allmond, S. Duric, R. Gujju Gurunadha, A. Ivanov, K. Kaadze, D. Kim, Y. Maravin, T. Mitchell, A. Modak, K. Nam, J. Natoli, D. Roy

Kansas State University, Manhattan, KS, USA

F. Rebassoo, D. Wright

Lawrence Livermore National Laboratory, Livermore, CA, USA

E. Adams, A. Baden, O. Baron, A. Belloni, S.C. Eno, N.J. Hadley, S. Jabeen, R.G. Kellogg, T. Koeth, Y. Lai, S. Lascio, A.C. Mignerey, S. Nabili, C. Palmer, C. Papageorgakis, M. Seidel, L. Wang, K. Wong

University of Maryland, College Park, MD, USA

D. Abercrombie, R. Bi, W. Busza, I.A. Cali, Y. Chen, M. D'Alfonso, J. Eysermans, C. Freer, G. Gomez-Ceballos, M. Goncharov, P. Harris, M. Hu, D. Kovalskyi, J. Krupa, Y.-J. Lee, K. Long, C. Mironov, C. Paus, D. Rankin, C. Roland, G. Roland, Z. Shi, G.S.F. Stephans, J. Wang, Z. Wang, B. Wyslouch

Massachusetts Institute of Technology, Cambridge, MA, USA

R.M. Chatterjee, B. Crossman, A. Evans, J. Hiltbrand, Sh. Jain, B.M. Joshi, C. Kapsiak, M. Krohn, Y. Kubota, J. Mans, M. Revering, R. Rusack, R. Saradhy, N. Schroeder, N. Strobbe, M.A. Wadud

University of Minnesota, Minneapolis, MN, USA

L.M. Cremaldi

University of Mississippi, Oxford, MS, USA

K. Bloom, M. Bryson, S. Chauhan, D.R. Claes, C. Fangmeier, L. Finco, F. Golf, C. Joo, I. Kravchenko, I. Reed, J.E. Siado, G.R. Snow [†], W. Tabb, A. Wightman, F. Yan, A.G. Zecchinelli

University of Nebraska-Lincoln, Lincoln, NE, USA

G. Agarwal, H. Bandyopadhyay, L. Hay, I. Iashvili, A. Kharchilava, C. McLean, M. Morris, D. Nguyen, J. Pekkanen, S. Rappoccio, A. Williams

State University of New York at Buffalo, Buffalo, NY, USA

G. Alverson, E. Barberis, Y. Haddad, Y. Han, A. Krishna, J. Li, J. Lidrych, G. Madigan, B. Marzocchi, D.M. Morse, V. Nguyen, T. Orimoto, A. Parker, L. Skinnari, A. Tishelman-Charny, T. Wamorkar, B. Wang, A. Wisecarver, D. Wood

Northeastern University, Boston, MA, USA

S. Bhattacharya, J. Bueghly, Z. Chen, A. Gilbert, T. Gunter, K.A. Hahn, Y. Liu, N. Odell, M.H. Schmitt, M. Velasco

Northwestern University, Evanston, IL, USA

R. Band, R. Bucci, M. Cremonesi, A. Das, R. Goldouzian, M. Hildreth, K. Hurtado Anampa, C. Jessop, K. Lannon, J. Lawrence, N. Loukas, L. Lutton, J. Mariano, N. Marinelli, I. Mcalister, T. McCauley, C. Mcgrady, K. Mohrman, C. Moore, Y. Musienko [13], H. Nelson, R. Ruchti, A. Townsend, M. Wayne, H. Yockey, M. Zarucki, L. Zygala

University of Notre Dame, Notre Dame, IN, USA

B. Bylsma, M. Carrigan, L.S. Durkin, B. Francis, C. Hill, A. Lesauvage, M. Nunez Ornelas, K. Wei, B.L. Winer, B.R. Yates

The Ohio State University, Columbus, OH, USA

F.M. Addesa, B. Bonham, P. Das, G. Dezoort, P. Elmer, A. Frankenthal, B. Greenberg, N. Haubrich, S. Higginbotham, A. Kalogeropoulos, G. Kopp, S. Kwan, D. Lange, D. Marlow, K. Mei, I. Ojalvo, J. Olsen, D. Stickland, C. Tully

Princeton University, Princeton, NJ, USA

S. Malik, S. Norberg

University of Puerto Rico, Mayaguez, PR, USA

A.S. Bakshi, V.E. Barnes, R. Chawla, S. Das, L. Gutay, M. Jones, A.W. Jung, D. Kondratyev, A.M. Koshy, M. Liu, G. Negro, N. Neumeister, G. Paspalaki, S. Piperov, A. Purohit, J.F. Schulte, M. Stojanovic, J. Thieman, F. Wang, R. Xiao, W. Xie

Purdue University, West Lafayette, IN, USA

J. Dolen, N. Parashar

Purdue University Northwest, Hammond, IN, USA

D. Acosta, A. Baty, T. Carnahan, M. Decaro, S. Dildick, K.M. Ecklund, P.J. Fernández Manteca, S. Freed, P. Gardner, F.J.M. Geurts, A. Kumar, W. Li, B.P. Padley, R. Redjimi, J. Rotter, W. Shi, S. Yang, E. Yigitbasi, L. Zhang [89], Y. Zhang, X. Zuo

Rice University, Houston, TX, USA

A. Bodek, P. de Barbaro, R. Demina, J.L. Dulemba, C. Fallon, T. Ferbel, M. Galanti, A. Garcia-Bellido, O. Hindrichs, A. Khukhunaishvili, E. Ranken, R. Taus, G.P. Van Onsem

University of Rochester, Rochester, NY, USA

K. Goulianos

The Rockefeller University, New York, NY, USA

B. Chiarito, J.P. Chou, Y. Gershtein, E. Halkiadakis, A. Hart, M. Heindl, O. Karacheban [24], I. Laflotte, A. Lath, R. Montalvo, K. Nash, M. Osherson, S. Salur, S. Schnetzer, S. Somalwar, R. Stone, S.A. Thayil, S. Thomas, H. Wang

Rutgers, The State University of New Jersey, Piscataway, NJ, USA

H. Acharya, A.G. Delannoy, S. Fiorendi, T. Holmes, E. Nibigira, S. Spanier

University of Tennessee, Knoxville, TN, USA

O. Bouhali [90], M. Dalchenko, A. Delgado, R. Eusebi, J. Gilmore, T. Huang, T. Kamon [91], H. Kim, S. Luo, S. Malhotra, R. Mueller, D. Overton, D. Rathjens, A. Safonov

Texas A&M University, College Station, TX, USA

N. Akchurin, J. Damgov, V. Hegde, K. Lamichhane, S.W. Lee, T. Mengke, S. Muthumuni, T. Peltola, I. Volobouev, Z. Wang, A. Whitbeck

Texas Tech University, Lubbock, TX, USA

E. Appelt, S. Greene, A. Gurrola, W. Johns, A. Melo, F. Romeo, P. Sheldon, S. Tuo, J. Velkovska, J. Viinikainen

Vanderbilt University, Nashville, TN, USA

B. Cardwell, B. Cox, G. Cummings, J. Hakala, R. Hirosky, M. Joyce, A. Ledovskoy, A. Li, C. Neu, C.E. Perez Lara, B. Tannenwald

University of Virginia, Charlottesville, VA, USA

P.E. Karchin, N. Poudyal

Wayne State University, Detroit, MI, USA

S. Banerjee, K. Black, T. Bose, S. Dasu, I. De Bruyn, P. Everaerts, C. Galloni, H. He, M. Herndon, A. Herve, C.K. Koraka, A. Lanaro, A. Loeliger, R. Loveless, J. Madhusudanan Sreekala, A. Mallampalli, A. Mohammadi, S. Mondal, G. Parida, D. Pinna, A. Savin, V. Shang, V. Sharma, W.H. Smith, D. Teague, H.F. Tsoi, W. Vetens

University of Wisconsin – Madison, Madison, WI, USA

S. Afanasiev, V. Andreev, Yu. Andreev, T. Aushev, M. Azarkin, A. Babaev, A. Belyaev, V. Blinov [92], E. Boos, V. Borshch, D. Budkouski, V. Bunichev, O. Bychkova, M. Chadeeva [92], V. Chekhovsky, A. Dermenev, T. Dimova [92], I. Dremin, M. Dubinin [82], L. Dudko, V. Epshteyn, A. Ershov, G. Gavrilov, V. Gavrilov, S. Gninenko, V. Golovtcov, N. Golubev, I. Golutvin, I. Gorbunov, A. Gribushin, V. Ivanchenko, Y. Ivanov, V. Kachanov, L. Kardapoltsev [92], V. Karjavine, A. Karneyeu, V. Kim [92], M. Kirakosyan, D. Kirpichnikov, M. Kirsanov, V. Klyukhin, O. Kodolova [93], D. Konstantinov, V. Korenkov, A. Kozyrev [92], N. Krasnikov, E. Kuznetsova [94], A. Lanev, P. Levchenko, A. Litomin, N. Lychkovskaya, V. Makarenko, A. Malakhov, V. Matveev [92], V. Murzin, A. Nikitenko [95], S. Obraztsov, V. Okhotnikov, A. Oskin, I. Ovtin [92], V. Palichik, P. Parygin, V. Perelygin, S. Petrushanko, G. Pivovarov, V. Popov, E. Popova, O. Radchenko [92], V. Rusinov, M. Savina, V. Savrin, V. Shalaev, S. Shmatov, S. Shulha, Y. Skovpen [92], S. Slabospitskii, V. Smirnov, D. Sosnov, A. Stepennov, V. Sulimov, E. Tcherniaev, A. Terkulov, O. Teryaev, I. Tlisova, M. Toms,

A. Toropin, L. Uvarov, A. Uzunian, E. Vlasov, A. Vorobyev, N. Voytishin, B.S. Yuldashev [96], A. Zarubin, I. Zhizhin, A. Zhokin

Authors affiliated with an institute or an international laboratory covered by a cooperation agreement with CERN

† Deceased.
[1] Also at Yerevan State University, Yerevan, Armenia.
[2] Also at TU Wien, Vienna, Austria.
[3] Also at Institute of Basic and Applied Sciences, Faculty of Engineering, Arab Academy for Science, Technology and Maritime Transport, Alexandria, Egypt.
[4] Also at Université Libre de Bruxelles, Bruxelles, Belgium.
[5] Also at Universidade Estadual de Campinas, Campinas, Brazil.
[6] Also at Federal University of Rio Grande do Sul, Porto Alegre, Brazil.
[7] Also at UFMS, Nova Andradina, Brazil.
[8] Also at The University of the State of Amazonas, Manaus, Brazil.
[9] Also at University of Chinese Academy of Sciences, Beijing, China.
[10] Also at Nanjing Normal University Department of Physics, Nanjing, China.
[11] Now at The University of Iowa, Iowa City, Iowa, USA.
[12] Also at University of Chinese Academy of Sciences, Beijing, China.
[13] Also at an institute or an international laboratory covered by a cooperation agreement with CERN.
[14] Also at Suez University, Suez, Egypt.
[15] Now at British University in Egypt, Cairo, Egypt.
[16] Also at Purdue University, West Lafayette, Indiana, USA.
[17] Also at Université de Haute Alsace, Mulhouse, France.
[18] Also at Department of Physics, Tsinghua University, Beijing, China.
[19] Also at Erzincan Binali Yildirim University, Erzincan, Turkey.
[20] Also at CERN, European Organization for Nuclear Research, Geneva, Switzerland.
[21] Also at University of Hamburg, Hamburg, Germany.
[22] Also at RWTH Aachen University, III. Physikalisches Institut A, Aachen, Germany.
[23] Also at Isfahan University of Technology, Isfahan, Iran.
[24] Also at Brandenburg University of Technology, Cottbus, Germany.
[25] Also at Forschungszentrum Jülich, Juelich, Germany.
[26] Also at Physics Department, Faculty of Science, Assiut University, Assiut, Egypt.
[27] Also at Karoly Robert Campus, MATE Institute of Technology, Gyongyos, Hungary.
[28] Also at Wigner Research Centre for Physics, Budapest, Hungary.
[29] Also at Institute of Physics, University of Debrecen, Debrecen, Hungary.
[30] Also at Institute of Nuclear Research ATOMKI, Debrecen, Hungary.
[31] Now at Universitatea Babes-Bolyai – Facultatea de Fizica, Cluj-Napoca, Romania.
[32] Also at Faculty of Informatics, University of Debrecen, Debrecen, Hungary.
[33] Also at Punjab Agricultural University, Ludhiana, India.
[34] Also at UPES – University of Petroleum and Energy Studies, Dehradun, India.
[35] Also at University of Visva-Bharati, Santiniketan, India.
[36] Also at University of Hyderabad, Hyderabad, India.
[37] Also at Indian Institute of Science (IISc), Bangalore, India.
[38] Also at Indian Institute of Technology (IIT), Mumbai, India.
[39] Also at IIT Bhubaneswar, Bhubaneswar, India.
[40] Also at Institute of Physics, Bhubaneswar, India.
[41] Also at Deutsches Elektronen-Synchrotron, Hamburg, Germany.
[42] Also at Sharif University of Technology, Tehran, Iran.
[43] Also at Department of Physics, University of Science and Technology of Mazandaran, Behshahr, Iran.
[44] Also at Helwan University, Cairo, Egypt.
[45] Also at Italian National Agency for New Technologies, Energy and Sustainable Economic Development, Bologna, Italy.
[46] Also at Centro Siciliano di Fisica Nucleare e di Struttura Della Materia, Catania, Italy.
[47] Also at Scuola Superiore Meridionale, Università di Napoli 'Federico II', Napoli, Italy.
[48] Also at Fermi National Accelerator Laboratory, Batavia, Illinois, USA.
[49] Also at Università di Napoli 'Federico II', Napoli, Italy.
[50] Also at Consiglio Nazionale delle Ricerche – Istituto Officina dei Materiali, Perugia, Italy.
[51] Also at Department of Applied Physics, Faculty of Science and Technology, Universiti Kebangsaan Malaysia, Bangi, Malaysia.
[52] Also at Consejo Nacional de Ciencia y Tecnología, Mexico City, Mexico.
[53] Also at IRFU, CEA, Université Paris-Saclay, Gif-sur-Yvette, France.
[54] Also at Faculty of Physics, University of Belgrade, Belgrade, Serbia.
[55] Also at Trincomalee Campus, Eastern University, Sri Lanka, Nilaveli, Sri Lanka.
[56] Also at INFN Sezione di Pavia, Università di Pavia, Pavia, Italy.
[57] Also at National and Kapodistrian University of Athens, Athens, Greece.
[58] Also at Ecole Polytechnique Fédérale Lausanne, Lausanne, Switzerland.
[59] Also at Universität Zürich, Zurich, Switzerland.
[60] Also at Stefan Meyer Institute for Subatomic Physics, Vienna, Austria.
[61] Also at Laboratoire d'Annecy-le-Vieux de Physique des Particules, IN2P3-CNRS, Annecy-le-Vieux, France.
[62] Also at Near East University, Research Center of Experimental Health Science, Mersin, Turkey.
[63] Also at Konya Technical University, Konya, Turkey.
[64] Also at Izmir Bakircay University, Izmir, Turkey.

[65] Also at Adiyaman University, Adiyaman, Turkey.
[66] Also at Necmettin Erbakan University, Konya, Turkey.
[67] Also at Bozok Universitetesi Rektörlügü, Yozgat, Turkey.
[68] Also at Marmara University, Istanbul, Turkey.
[69] Also at Milli Savunma University, Istanbul, Turkey.
[70] Also at Kafkas University, Kars, Turkey.
[71] Also at Hacettepe University, Ankara, Turkey.
[72] Also at Istanbul University – Cerrahpasa, Faculty of Engineering, Istanbul, Turkey.
[73] Also at Yildiz Technical University, Istanbul, Turkey.
[74] Also at Vrije Universiteit Brussel, Brussel, Belgium.
[75] Also at School of Physics and Astronomy, University of Southampton, Southampton, United Kingdom.
[76] Also at University of Bristol, Bristol, United Kingdom.
[77] Also at IPPP Durham University, Durham, United Kingdom.
[78] Also at Monash University, Faculty of Science, Clayton, Australia.
[79] Also at Università di Torino, Torino, Italy.
[80] Also at Bethel University, St. Paul, Minnesota, USA.
[81] Also at Karamanoğlu Mehmetbey University, Karaman, Turkey.
[82] Also at California Institute of Technology, Pasadena, California, USA.
[83] Also at United States Naval Academy, Annapolis, Maryland, USA.
[84] Also at Ain Shams University, Cairo, Egypt.
[85] Also at Bingol University, Bingol, Turkey.
[86] Also at Georgian Technical University, Tbilisi, Georgia.
[87] Also at Sinop University, Sinop, Turkey.
[88] Also at Erciyes University, Kayseri, Turkey.
[89] Also at Institute of Modern Physics and Key Laboratory of Nuclear Physics and Ion-beam Application (MOE) – Fudan University, Shanghai, China.
[90] Also at Texas A&M University at Qatar, Doha, Qatar.
[91] Also at Kyungpook National University, Daegu, Republic of Korea.
[92] Also at another institute or international laboratory covered by a cooperation agreement with CERN.
[93] Also at Yerevan Physics Institute, Yerevan, Armenia.
[94] Now at University of Florida, Gainesville, Florida, USA.
[95] Also at Imperial College, London, United Kingdom.
[96] Also at Institute of Nuclear Physics of the Uzbekistan Academy of Sciences, Tashkent, Uzbekistan.